Enhancing Spectral Efficiency of Short-Packet Communications in STAR-RIS-Assisted SWIPT MIMO-NOMA Systems with Deep Learning

Ridho Hendra Yoga Perdana, *Graduate Student Member, IEEE,* Toan-Van Nguyen, *Member, IEEE,* Yushintia Pramitarini, *Graduate Student Member, IEEE,* Duy H. N. Nguyen, *Senior Member, IEEE,* and Beongku An *Senior Member, IEEE,*

***Abstract*—This paper proposes an adaptive user grouping (AUG) scheme for short-packet communication (SPC) in simultaneous transmitting and reflecting (STAR)-reconfigurable intelligent surface (RIS)-assisted multiple-input multiple-output (MIMO)-non-orthogonal multiple access (NOMA) systems with SWIPT. The information users with different channel conditions are optimally grouped while the energy user harvests the energy from the base station. Besides that, multiple STAR-RISs are deployed to assist the information users in improving the quality of received signals. We formulate the spectral efficiency (SE) maximization of the considered system to optimize the linear precoding matrix, phase shift of the reflection and transmission at STAR-RIS, energy beamforming matrix, and grouping variables. The formulated problem leads to a mixed binary integer programming which is challenging to solve optimally. To tackle this problem, we first relax the integer variable to be continuous and decouple the relaxed problem into two subproblems to alternately tackle the phase shift and beamforming parts. We then propose bisection search and low-complexity iterative algorithms to solve the phase shift and beamforming subproblems with guaranteed convergence at a relative optimum of each subproblem. Towards real-time optimization, we develop a convolutional neural network (CNN) to achieve the optimal solution of the relaxed problem via a quick-inference process. Numerical results demonstrate a SE improvement of 46% in the AUG scheme over the random user grouping one and 78% over the non-user grouping under various settings. Furthermore, the developed CNN model predicts optimal phase shift variables and beamforming matrices with high accuracy compared to conventional methods but in a shorter time.**

***Index Terms*—Convolutional neural networks, energy harvesting, MIMO, NOMA, non-convex optimization, short-packet communication, spectral efficiency, user grouping, STAR-RIS.**

The work of R. H. Y. Perdana, Y. Pramitarini, and B. An was supported by National Research Foundation of Korea (NRF) grant funded by the Korea government (MSIT) (NRF-2022R1A2B5B01001190). The work of Toan-Van Nguyen and Duy H. N. Nguyen was supported by the U.S. National Science Foundation under grants ECCS-2146436, CCF-2225576, and CCF-2322190. *(Corresponding author: Beongku An.)*

Ridho Hendra Yoga Perdana and Yushintia Pramitarini are with the Department of Software and Communications Engineering, Graduate School, Hongik University, Sejong 30016, Republic of Korea (e-mails: mail.rhyp@gmail.com; yushintia@gmail.com).

Toan-Van Nguyen and Duy H. N. Nguyen are with the Department of Electrical and Computer Engineering, San Diego State University (e-mails: vannguyentoan@gmail.com; duy.nguyen@sdsu.edu).

Beongku An (Corresponding author) is with the Department of Software and Communications Engineering, Hongik University, Sejong 30016, Republic of Korea (e-mail: beongku@hongik.ac.kr).

I. Introduction

The challenges in the fifth generation (5G) and beyond 5G wireless communication network are not only higher spectral efficiency (SE) but also ultra-reliable and low-latency communications (URLLCs) for the Internet-of-Things (IoT)-enable beyond 5G networks [1]. One of the techniques in URLLC is short-packet communication (SPC), where it can provide high reliability ($\geq$ 90%) and low latency communications ($\simeq$ 1ms) [2]. SPC applying for multiple-input multiple-output (MIMO)-non-orthogonal multiple access (NOMA) can improve communication reliability while achieving high spectral efficiency and extending the network coverage [3]. Nevertheless, communication systems functioning under finite block length encounter substantial challenges concerning information-theoretic performance evaluation and pilot transmission perspectives [4], wherein the applicability of the Shannon capacity formula becomes invalidated.

User grouping or user pairing is one of the effective strategies to achieve the benefits of NOMA in supporting large connectivity and high data rates in IoT-enabling beyond 5G networks. Nevertheless, the load of systems becomes heavier as the number of users on the network increases. To address this issue, recent studies have proposed various user pairing algorithms to improve SE and energy efficiency (EE) of NOMA systems, for example, scheduling algorithms [5], hybrid user pairing [6], and adaptive user pairing [7]. Moreover, the SE performance also improved when the reconfigurable intelligent surfaces (RIS) were implemented in the NOMA system [7]. Thus, implementing the user pairing is a promising approach to improve the SE performance in the system.

To meet requirements for wider coverage area and high SE, RIS has attracted growing attention in recent years because of its ability to flexibly configure the wireless signal propagation environment through the amplitude and phase shift of each element, thus improving the SE performance of wireless systems [7]. However, the traditional RIS is only designed with a limited reflection area (180°), therefore, it cannot reach users located behind the reflection area. To tackle this problem, the authors in [8] introduced a simultaneously transmitting and reflecting reconfigurable intelligent surface (STAR-RIS) to achieve 360° wireless coverage, which improves the SE performance by leveraging both surfaces. Consequently, researchers have delved into STAR-RIS, combining it with var-

ious multiple access techniques such as rate splitting multiple access (RSMA) [9] or NOMA [10] to further enhance the SE and EE of IoT and 5G systems.

A. Literature Survey

In addition to addressing bandwidth constraints and realizing URLLCs to support IoT-enabling beyond 5G networks, SPC is considered as a promising approach to improve reliability and latency communications [11]. The authors in [11] studied a novel cooperative beamforming relay selection scheme to improve high-reliable transmission in SPC multi-hop networks with energy harvesting (EH). Additionally, deep learning (DL)-based optimization was proposed to improve end-to-end throughput in the system. The authors in [12] proposed the optimal selection scheme to improve the reliability of simultaneous wireless information and power transfer (SWIPT) under power-splitting and time-switching protocols with finite blocklength codes. In [13], the authors analyzed and optimized the RIS-assisted SPC supported by wireless energy transfer (WET) and wireless information transfer (WIT) phases.

Regarding the improvement of the SE performance by user grouping, the authors in [5] studied the paired scheduling algorithm and user grouping, which simultaneously paired the selected user groups and scheduled suitable user groups for data transmission in MIMO-NOMA networks. The authors in [6] studied the hybrid user pairing scheme and developed an iterative algorithm to solve the EE and SE problems in multiple-input single-output (MISO)-NOMA networks with SWIPT. The authors in [14] considered the cooperative NOMA-based user pairing to provide better BLER and latency in the URLLC. To improve SE, a DL-based adaptive user pairing in multi-RIS-aided massive MIMO-NOMA networks was proposed in [7].

On the other hand, RIS systems with SPC have been extensively studied [15], [16]. The performance analysis of RIS-aided SPC was studied in [15], focusing on the average data rate and decoding error probability, which was potentially applied for factory automation scenarios. Due to the traditional RIS only having a limited reflection area, the authors in [16] analyzed the STAR-RIS and NOMA systems, which can serve 360^o wireless coverage under finite blocklength. The authors in [17] derived the closed-form expression for the average block error rate (BLER) and achievable rate in STAR-RIS-enable SPC-NOMA systems with the discrete phase shift alignment to reduce the STAR-RIS implementation cost. The authors in [9] studied the downlink STAR-RIS-RSMA system by considering ES and mode switching (MS) configurations of the STAR-RIS. The joint optimization problem of phase shift and beamforming design in multi-user MISO STAR-RIS-assisted NOMA network was addressed to achieve the maximum downlink energy efficiency [18]. The authors in [8] studied the IA method and DL-based framework to improve SE in massive MIMO-NOMA systems with STAR-RIS.

Furthermore, the number of users in the 5G and beyond 5G wireless network is growing rapidly [19]. Consequently, several problems arise, such as channel estimation resource allocation and channel coding [20], which are difficult to solve using conventional methods, whereas the DL-based design can enhance system performance in the URLLC system [21]. Moreover, applying a DL-based approach can reduce the processing time and complexity in determining block-error rate (BLER) to maximize throughput while ensuring link reliability [22]. Meanwhile, Nguyen *et al.* in [11] developed a convolution neural network (CNN) framework to maximize end-to-end throughput and optimal channel uses for SPC in the multi-hop networks with WET. However, the aforementioned works on DL in the URLLC communication have not considered the STAR-RIS to enhance large and seamless connectivity.

B. Motivations and Contributions

Most of the aforementioned works mainly focused on the SPC combining with SWIPT or WET [12], [13], user grouping [5], [6], and STAR-RIS [9], [16], [17] in MIMO-NOMA systems. However, the following fundamental questions still need to be discussed and answered.

- *From the practical under-deployment perspective, how the system can effectively group users when the number of near and far users is different?*
- *Considering spectral efficiency maximization (SEM) problem for SPC in STAR-RIS-assisted MIMO-NOMA systems with SWIPT, how to achieve the optimal solution of beamforming design and phase shift at the STAR-RIS when considering the users grouping?*
- *Regarding the number of users and STAR-RISs increasing for SPC in STAR-RIS-assisted MIMO-NOMA system with SWIPT, how to efficiently obtain the optimal solution to address the SEM problem within a short time?*

Against the above background, we consider SPCs in a downlink SWIPT MIMO-NOMA system, where the direct link is only available from the BS to energy users while the information users are blocked from the BS because of deep shadowing. Integrating various cutting-edge technologies such as MIMO-NOMA, SPC, STAR-RIS, and SWIPT is pivotal for advancing the capabilities of 5G and beyond networks. The benefit of combining them significantly improves SE performance, which enables massive connectivity, low latency, and high-reliability communication, while the DL approach allows the considered system to perform real-time resource allocation for practical applications demanding high reliability and low latency such as factory automation, IoT systems in hard-to-reach environments, smart transportation systems, and healthcare monitoring systems. In addition, by applying SWIPT, the IoT devices can harvest the energy from BS, enabling them to maintain seamless connectivity and function reliably over time [23]. This dual capability is especially beneficial in IoT applications where devices are often situated in hard-to-reach areas or are required to function over extended periods without maintenance. Multiple STAR-RISs are deployed between BS and information users to improve the received signal quality. Moreover, the novel adaptive user grouping (AUG) scheme is proposed to enhance SE performance by selecting the optimal information user for grouping. The proposed scheme allows multiple users to share a single resource block, which effectively reduces communication latency [2]. Furthermore, several challenges need to be addressed along

with the proposed AUG scheme as follows. *1)* The spectral efficiency expression under SPCs is shown as a complicated function of the blocklength and a non-convex [11], making its optimization design in STAR-RIS-assisted MIMO-NOMA system with SWIPT more challenging to solve; *2)* The phase shift of STAR-RIS and user grouping variables contain discrete values, making the spectral efficiency maximization belong to the class mixed-integer non-linear programming class; *3)* Due to the high non-convex characteristics, the formulated problem is still highly non-convex even though it is divided into subproblems; *4)* Increasing the number of users and STAR-RISs, the adaptive user grouping approach with NOMA to achieve optimal solutions will take a longer time due to the high computational complexity.

To address the challenges above, we develop a low-complexity iterative algorithm based on the inner approximation (IA) method, which solves a second-order cone (SOC) program in every iteration, where the feasibility set in every step contains the previous step and is part of a subset of the feasibility set of the original formulated problem. To effectively tackle the SE optimization problem, our approach introduces innovative transformations that refine the problem into a more tractable form without loss of generality. The approach systematically navigates the complex optimization problem by decomposing the problem into more tractable subproblems, specifically focusing on phase shift and beamforming optimizations. The iterative algorithm based on the IA method finds the optimal solutions of the linear precoding matrix, the energy beamforming matrix, and the phase shifts at STAR-RIS, ensuring convergence to maximize SE while adhering to the constraints imposed by power budget, energy harvesting, grouping user and phase shift of the STAR-RIS. This method illustrates a comprehensive strategy for solving the formulated problem with low computational complexity to achieve optimal solutions. The main contributions of the paper can be summarized as follows:

- We propose an AUG scheme with SPC to improve SE performance in STAR-RIS-assisted MIMO-NOMA systems with SWIPT, which has not been studied in [10]. Particularly, two information users in different zones are optimally grouped, which can reduce intra-pair interference, while the energy users harvest the energy from the base station (BS). With the benefits of refracting and reflecting incident waves to the desired positions of STAR-RIS, the signal quality of information users can be improved. We also investigate the random user grouping (RUG) and non-user grouping (NUG) as benchmark schemes for comparison.
- We formulate the problem of spectral efficiency maximization subject to total power, user grouping, and phase shift at STAR-RIS constraints. This problem is non-convex with mixed-integer constraints, which is very challenging to solve optimally due to the problem belonging to the mixed-integer non-convex programming class. By following the inner approximation method [24], we first relax the integer (user grouping and phase shift) variables to be continuous, then decouple the relaxed problem into phase shift and beamforming optimization problems. We propose a bisection algorithm to tackle the phase shift problem, and then based on the optimal solution of phase shift, we solve the beamforming problem by transforming it into a more tractable non-convex equivalent form. We then develop an iterative algorithm with low computational complexity to solve the beamforming problem and convergence at a relative optimum.
- Towards real-time optimization, we develop a DL framework based on the CNN model to predict the optimal solution of the linear precoding matrix, phase shift at STAR-RIS, energy beamforming matrix and grouping variable based on the developed algorithm. We design the CNN model with multiple convolutional layers connected with structural multiscale accumulation to effectively collect precise features to accurately predict the linear precoding matrix, phase shift at STAR-RIS, energy beamforming matrix, and grouping variables in real-time.
- Simulation results show the SE improvement of the proposed AUG scheme. Furthermore, the AUG scheme outperforms the RUG and NUG schemes due to the two information users being optimally grouped. Moreover, the designed CNN model can predict the same optimal solution as the conventional method but in a very short time so that it can enable real-time decision-making tasks in 5G and beyond 5G wireless communication networks.

Notation: Matrices, vectors, and scalars are denoted by bold-face upper-case, bold-face lower-case, and lower-case, respectively. $(\cdot)^H$, $(\cdot)^*$, $|\cdot|$ and $\|\cdot\|$ are transpose conjugate, complex conjugate, absolute, and Frobenius norm values, respectively. $\mathbb{R}$ and $\mathbb{C}$ are the set of real and complex numbers, respectively. $\mathbf{I}$ is $M_{\rm BS} \times M_{\rm u}$ matrix identity, $\mathcal{CN}(x,u)$ is circularly symmetric complex Gaussian distribution with covariance matrix u and mean x. $\mathrm{Trace}(\mathbf{V})$ is the trace of matrix $\mathbf{V}$ while $\Re$ denote real parts numbers. We summarize the main variable/notations in Sections II, III, IV in Table I.

II. System Model

A. System Description

Let us consider a downlink multiple user MIMO-NOMA system assisted multiple STAR-RISs with SWIPT, where a BS is deployed to serve simultaneously a set of energy users $\mathcal{Q} = \{\mathsf{E}_q\}_{q=1}^{Q}$, a set of near information user $\mathcal{N} = \{\mathrm{ID}_n\}_{n=1}^{N}$ and a set of far information user $\mathcal{F} = \{\mathrm{ID}_f\}_{f=1}^{F}$ via a set of STAR-RISs $\mathcal{K} = \{\mathsf{R}_k\}_{k=1}^{K}$ using NOMA transmission, as illustrated in Fig. 1. We assume the BS is equipped with $M_{\rm BS} > 1$ antennas while energy users, near and far information users are equipped with single, $M_n > 1$ and $M_f > 1$ antennas. The STAR-RIS is divided into two element parts with $L = \{L_r, L_t\}$, where $L_r \geq 1$ for reflection mode and $L_t \geq 1$ for transmission mode, respectively. We assume that the network is divided into three zones, where zone 1 is the nearest disc with an inner radius of d_1, and users in zone 1 communicate with the BS through line-of-sight (LoS) without any obstacles. Zone 3 is an annular area with an outer radius of d_3, while zone 2 is an area located between zones 1 and 3 with a radius of d_2. Users located in zones 2 and 3 cannot communicate directly with the BS through LoS since there

TABLE I
SUMMARY OF THE VARIABLES/NOTATIONS

variables/Notations	Descriptions
$\mathsf{E}_q, \mathsf{R}_k, \mathrm{ID}_n, \mathrm{ID}_f$	Energy user, STAR-RIS, near and far information users
Q, K, N, F	Number of energy users, STAR-RISs, near and far information users
$M_{\mathrm{BS}}, M_n, M_f$	Number of antennas at BS, near and far information users
L_r, L_t	Number of reflection and transmission elements at STAR-RIS
$\mathbf{\Theta}_{\mathsf{R}_k}, \mathbf{\Psi}_{\mathsf{R}_k}$	Phase shift matrix of reflecting and transmitting elements
$\kappa_{L_r}, \kappa_{L_t}$	amplitude coefficient of reflecting and transmitting elements
$\mathbf{H}, \mathbf{h}$	Channel coefficient matrix and vector
$\mathbf{y}_q, \mathbf{y}_n, \mathbf{y}_f$	Received signal at E_q, ID_n and ID_f
$\gamma_b^{\varsigma p}, \gamma_p^{\varsigma p}$	The SINR at ID_b and ID_p without grouping elements
$\gamma_b^{\mathrm{AUG}}, \gamma_p^{\mathrm{AUG}}$	The SINR at ID_b and ID_p including grouping elements
$\mathbf{P}$	User grouping matrix
$\mathbf{r}, \boldsymbol{\zeta}$	Auxiliary variable for soft data rates and SINR
$\mathbf{\Lambda}$	Auxiliary variable for $\mathbf{\Lambda} \triangleq \{\Lambda_{b,p} \geq 0\}$ which satisfies the convex constraint $\Lambda_{n,f'} \geq \lvert\hat{\mathbf{H}}_{\mathrm{B},b}(\mathbf{\Theta}_{\mathsf{R}_k})\mathbf{W}_b\rvert^2$
A, ϖ_b, ϖ_p	Number of blocklength, instantaneous BLER at ID_b and ID_p

are obstacles between zones 1 and 2. The BS is located in the center of the cell, while energy users, near and far information users are uniformly deployed at zones 1, 2, and 3, respectively. And also, the STAR-RIS deployed between zones 2 and 3 to help BS can communicate with information users. Thus, near and far information users are located in front and behind STAR-RIS. Moreover, there are no direct links from BS to near and far information users due to the obstacles. It is important to note that different channel conditions between ID_n and ID_f potentially make a user grouping at the same STAR-RIS for NOMA transmission [6]. Besides, since energy users have limited power supplies and are located in zone 1, they can harvest energy from BS and store it in their local batteries for future processing [6]. We assume that BS and all users already know the networks' channel state information (CSI) and all channels except the channel between BS and STAR-RIS experience quasi-static independent identically distributed (i.i.d.) Rayleigh fading[1]. Without loss of generality, we also assume each element (reflection and transmission) of STAR-RIS to be ideal without energy consumption, thus we set the amplitude coefficient of reflecting elements $\kappa_{L_r} = 1$ and transmitting elements $\kappa_{L_t} = 1$ [30].

[1]In practice, the wireless transmission between the BS and energy users and transmissions from the STAR-RIS to information users can be subject to uncertainties, including isotropic scattering and blocking from surrounding environments such as leaves, ground surfaces and walls, thus Rayleigh fading is utilized to model this transmission channel [25], [26]. Meanwhile, transmissions from BS to STAR-RIS always maintain LoS conditions, and Rician fading is utilized to model this transmission channel [27]. Additionally, the Rayleigh fading is the worst wireless fading channel compared to the Rician and Nakagami ones, and if the system can operate well under the Rayleigh fading channels, it also works well with other fading channels. For this reason, Rayleigh fading channels have been considered in various works of STAR-RIS-Assisted MIMO-NOMA systems [17], [28], [29]

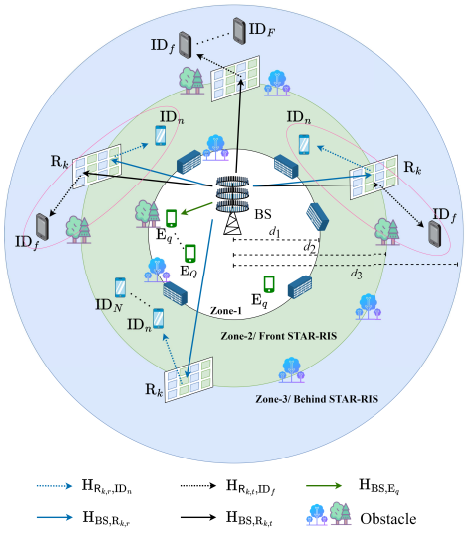

Fig. 1. Illustration of the proposed MIMO-NOMA systems with multiple STAR-RISs and SWIPT.

B. Channel Model and Energy Harvesting Processes

In our system model, spatial transmit beamforming is combined with NOMA transmission to serve multiple users concurrently on the same resource block regarding time, frequency, and spreading code. The BS delivers power to Q energy users via an energy beamforming matrix and simultaneously transmits information messages to information users (near and far) through information beamforming. Thus, the superimposed signal transmitted from BS to users as $\mathbf{X} = \mathbf{V}_q + \sum_{n\in\mathcal{N}} \mathbf{W}_n \varsigma_n + \sum_{f\in\mathcal{F}} \mathbf{W}_f \varsigma_f$, where $\mathbf{V}_q \sim \mathcal{CN}(0, \mathbf{V}\mathbf{V}^{\mathrm{H}})$, with $\mathbf{V} \in \mathbb{C}^{M_{\mathrm{BS}}\times\bar{Q}}$, is the energy beamforming matrix for Q energy users, where $\bar{Q} \leq \min(M_{\mathrm{BS}}, Q)$; $\mathbf{W}_n \in \mathbb{C}^{M_{\mathrm{BS}}\times d}$ and $\mathbf{W}_f \in \mathbb{C}^{M_{\mathrm{BS}}\times d}$ denote the information beamforming matrices for ID_n and ID_f, respectively; $\varsigma_n \in \mathbb{C}^{d\times 1}$ and $\varsigma_f \in \mathbb{C}^{d\times 1}$ are data signals intended for ID_n and ID_f, respectively; and d is the number of data streams transmitted for each information user $(\mathrm{ID}_n, \mathrm{ID}_f)$, where $1 \leq d \leq \min\{M_{\mathrm{BS}}, M_n, M_f\}$ for ID_n and ID_f.

The received signal at E_q, ID_n and ID_f can be expressed, respectively, as

$$\mathbf{y}_q = \mathbf{h}_{\mathrm{BS},\mathrm{E}_q}^H \mathbf{V}_q + \sum_{n\in\mathcal{N}} \mathbf{h}_{\mathrm{BS},\mathrm{E}_q}^H \mathbf{W}_n \varsigma_n + \sum_{f\in\mathcal{F}} \mathbf{h}_{\mathrm{BS},\mathrm{E}_q}^H \mathbf{W}_f \varsigma_f + \mathbf{n}_q, \tag{1}$$

$$\mathbf{y}_n = \sum_{n'\in\mathcal{N}\setminus\{n\}} \hat{\mathbf{H}}_{\mathrm{B},n}(\mathbf{\Theta}_{\mathsf{R}_k})\mathbf{W}_{n'}\varsigma_{n'} + \sum_{f\in\mathcal{F}} \hat{\mathbf{H}}_{\mathrm{B},n}(\mathbf{\Theta}_{\mathsf{R}_k})\mathbf{W}_f\varsigma_f + \hat{\mathbf{H}}_{\mathrm{B},n}(\mathbf{\Theta}_{\mathsf{R}_k})\mathbf{V}_q + \hat{\mathbf{H}}_{\mathrm{B},n}(\mathbf{\Theta}_{\mathsf{R}_k})\mathbf{W}_n\varsigma_n + \mathbf{n}_n, \tag{2}$$

$$\mathbf{y}_f = \sum_{f'\in\mathcal{F}\setminus\{f\}} \hat{\mathbf{H}}_{\mathrm{B},f}(\mathbf{\Psi}_{\mathsf{R}_k})\mathbf{W}_{f'}\varsigma_{f'} + \sum_{n\in\mathcal{N}} \hat{\mathbf{H}}_{\mathrm{B},f}(\mathbf{\Psi}_{\mathsf{R}_k})\mathbf{W}_n\varsigma_n + \hat{\mathbf{H}}_{\mathrm{B},f}(\mathbf{\Psi}_{\mathsf{R}_k})\mathbf{V}_q + \hat{\mathbf{H}}_{\mathrm{B},f}(\mathbf{\Psi}_{\mathsf{R}_k})\mathbf{W}_f\varsigma_f + \mathbf{n}_f, \tag{3}$$

where $\hat{\mathbf{H}}_{\mathrm{B},n}(\mathbf{\Theta}_{\mathsf{R}_k}) \triangleq \sum_{k\in\mathcal{K}} \mathbf{H}_{\mathsf{R}_{k,r},\mathrm{ID}_n} \mathbf{\Theta}_{\mathsf{R}_k} \mathbf{H}_{\mathrm{BS},\mathsf{R}_{k,r}}$, $\hat{\mathbf{H}}_{\mathrm{B},f}(\mathbf{\Psi}_{\mathsf{R}_k}) \triangleq \sum_{k\in\mathcal{K}} \mathbf{H}_{\mathsf{R}_{k,t},\mathrm{ID}_f} \mathbf{\Psi}_{\mathsf{R}_k} \mathbf{H}_{\mathrm{BS},\mathsf{R}_{k,t}}$, $\mathbf{H}_{\mathsf{R}_{k,r},\mathrm{ID}_n} \in \mathbb{C}^{L_r\times M_n}$, $\mathbf{H}_{\mathsf{R}_{k,t},\mathrm{ID}_f} \in \mathbb{C}^{L_t\times M_f}$, $\mathbf{H}_{\mathrm{BS},\mathsf{R}_{k,r}} \in \mathbb{C}^{L_r\times M_{\mathrm{BS}}}$ and $\mathbf{H}_{\mathrm{BS},\mathsf{R}_{k,t}} \in \mathbb{C}^{L_t\times M_{\mathrm{BS}}}$ denote the channel coefficient matrices from k-th STAR-RIS with reflection element $\mathsf{R}_{k,r}$ to

n-th near information user ID_n, from k-th STAR-RIS with transmission element $\mathsf{R}_{k,t}$ to f-th far information user ID_f, channel coefficient matrices from BS to k-th STAR-RIS with reflection element $\mathsf{R}_{k,r}$ and k-th STAR-RIS with transmission element $\mathsf{R}_{k,r}$, respectively. $\mathbf{h}_{\mathrm{BS},\mathrm{E}_q} \in \mathbb{C}^{M_{\mathrm{BS}}\times 1}$ denotes the channel coefficient vector from BS to E_q. $\mathbf{\Theta}_{\mathsf{R}_k}$ denotes the k-th STAR-RIS with reflection with diagonal matrix being $\mathbf{\Theta}_{\mathsf{R}_k} = \mathrm{diag}(\kappa_1\phi_{k,1}, \kappa_2\phi_{k,2}, \cdots, \kappa_{L_r}\phi_{k,L_r})$, where $\phi_{k,L_r} = e^{j\theta_{k,L_r}}$ with $\theta_{k,L_r} \in (0, 2\pi]$. While $\mathbf{\Psi}_{\mathsf{R}_k}$ denotes k-th STAR-RIS with transmission element with diagonal matrix being $\mathbf{\Psi}_{\mathsf{R}_k} = \mathrm{diag}(\kappa_1\psi_{k,1}, \kappa_2\psi_{k,2}, \cdots, \kappa_{L_r}\psi_{k,L_t})$, where $\psi_{k,L_t} = e^{j\delta_{k,L_r}}$ with $\delta_{k,L_r} \in (0, 2\pi]$. $\mathbf{n} \in \{\mathbf{n}_q, \mathbf{n}_n, \mathbf{n}_f\}$ denote the additive white Gaussian noise of E_q, ID_n and ID_f, respectively, where $\mathbf{n} \sim \mathcal{CN}(\mathbf{0}, \mathbf{I}\sigma^2)$, with $\sigma^2 \in \{\sigma_q^2, \sigma_n^2, \sigma_f^2\}$ of $\mathsf{E}_q, \mathrm{ID}_n$ and ID_f, respectively, and zero mean. The channel coefficient matrix can be modeled as $\mathbf{H} = \sqrt{\rho_h}[\tilde{\mathbf{h}}_1, \cdots, \tilde{\mathbf{h}}_i]$, where $\mathbf{H} \in \{\mathbf{H}_{\mathrm{BS},\mathsf{R}_{k,r}}, \mathbf{H}_{\mathrm{BS},\mathsf{R}_{k,t}}, \mathbf{H}_{\mathsf{R}_{k,r},\mathrm{ID}_n}, \mathbf{H}_{\mathsf{R}_{k,t},\mathrm{ID}_f}\}$, and each $\tilde{\mathbf{h}}_i$ is a small-scale fading vector. Similarly, the channel coefficient vector $\mathbf{h}$ is modeled as $\mathbf{h} = \sqrt{\rho_h}\tilde{\mathbf{h}}$ with $\mathbf{h} \in \{\mathbf{h}_{\mathrm{BS},\mathrm{E}_q}\}$, where ρ_h is the large-scale fading. Taking into account large-scale fading, ρ_h can be modeled as $\rho_h = \mathcal{L}(d_{\mathsf{a}\to\mathsf{b}}/d_0)^{-\sigma_{\mathrm{PL}}}$, where $d_{\mathsf{a}\to\mathsf{b}}$, σ_{PL}, d_0 and $\mathcal{L}$ present the distance (in meter) between a and b with $\mathsf{a} \in \{\mathrm{BS}, \mathsf{R}_k\}, \mathsf{b} \in \{\mathsf{R}_k, \mathrm{ID}_n, \mathrm{ID}_f\}$, the pathloss exponent, the reference distance, and the measured pathloss at d_0, respectively [11]. The small scale fading has i.i.d. $\mathcal{CN} \sim (0, 1)$ elements. Due to the LoS transmission links between the BS and the STAR-RIS, the small-scale fading can be characterized by the Rician fading model, whose all elements are both i.i.d. and satisfy $\tilde{h}_{\mathrm{BS},\mathsf{R}_k} = \sqrt{\frac{\mathsf{k}}{\mathsf{k}+1}}\bar{h}_{\mathrm{BS},\mathsf{R}_k} + \sqrt{\frac{1}{\mathsf{k}+1}}\hat{h}_{\mathrm{BS},\mathsf{R}_k}$, where $|\bar{h}_{\mathrm{BS},\mathsf{R}_k}| = 1$ is LoS component, $\hat{h}_{\mathrm{BS},\mathsf{R}_k} \sim \mathcal{CN}(0, 1)$ is NLoS component, and k is the Rician factor of $\tilde{\mathbf{h}}$ [31]. We consider discrete phase shifts at each reflecting/transmitting element of the STAR-RIS while the number of phase shifts is limited by phase shift resolution. The number of bits to quantize the continuous phase shift as $b_r^q = 8$, and the phase shift resolution at k-th STAR-RIS is $\mathsf{Res}_k \triangleq 2^{b_r^q}$ [30]. From (1), the radio frequency (RF) power at E_q for input of EH circuits can be expressed as [32]

$$\mathrm{E}_q(\mathbf{V}, \mathbf{W}) = \|\mathbf{h}_{\mathrm{BS},\mathrm{E}_q}^H \mathbf{V}_q\|^2 + \sum_{n\in\mathcal{N}} |\mathbf{h}_{\mathrm{BS},\mathrm{E}_q}^H \mathbf{W}_n|^2 + \sum_{f\in\mathcal{F}} |\mathbf{h}_{\mathrm{BS},\mathrm{E}_q}^H \mathbf{W}_f|^2. \quad (4)$$

To reflect the practical EH characteristics, we consider the non-linear WET at EH circuits, where the model of non-linear-energy harvesting (NL-EH) at E_q can be expressed as [32]

$$\mathrm{E}_q^{\mathrm{NL}}(\mathbf{V}, \mathbf{W}) = (\delta_q - \bar{P}_q\Omega_q)(1 - \Omega_q)^{-1}, \quad (5)$$

where $\delta_q = \bar{P}_q/(1 + \exp(-a_q(\mathrm{E}_q(\mathbf{V}, \mathbf{W}) - b_q)))$, $\bar{P}_q$ denotes the maximum energy harvested at E_q at saturation state of the EH circuit, a_q and b_q are constant parameters of the non-linear EH model such as hardware limitations (resistance, capacitance, etc.), and $\Omega_q = 1/(1 + \exp(a_q b_q))$.

C. Adaptive User Grouping Beamforming Scheme

In the proposed scheme, due to different channel conditions between ID_n in zone 2 and ID_f in zone 3, ID_n is potentially grouped with ID_f. Once they are in groups, ID_n/ID_f with good channel condition uses the successive interference cancellation (SIC) to decode ID_n's/ID_f's message and sequentially subtract it to get its own message, while ID_f can directly decode its own messages based on NOMA principle. Moreover, the multiple STAR-RISs can reflect/transmit by focusing the beamforming signal from BS to ID_n and ID_f to improve the signal quality of both users simultaneously. When the number of users in zone 2 is different from that of zone 3 (i.e., $\mathcal{N} \neq \mathcal{F}$), or when ID_n and ID_f are not belong to any group, the remaining users $|\mathcal{N} - \mathcal{F}|$ cannot be group and communicate directly to the BS using STAR-RIS with reflecting element for ID_n or transmission element for ID_f without using NOMA. Due to its simplicity for practical implementation, grouping two users has been widely studied [6], [33]. The benefit of the proposed scheme is low signal processing since the near information user is required to decode and subtract the signal of one far information user in one iteration. It should be noted that in the NUG scheme, the near information user requires many iterations to decode and subtract signals of all far information users to perform SIC, so it has a high signal processing [34]. In practice, when the channel conditions between two users in a group are not different, NOMA transmission may become inefficient [35]. Therefore, in the AUG scheme, the user with better ID_b and poorer ID_p channel conditions can be grouped if and only if the measure performance is improved. To implement it, we introduce a new grouping matrix $\mathbf{P} \in \mathbb{R}^{N\times F}$ with each element being expressed as

$$[\mathbf{P}]_{nf} = \begin{cases} 1, & \text{if } \mathrm{ID}_b \text{ and } \mathrm{ID}_p \text{ is grouped,} \\ 0, & \text{if } \mathrm{ID}_b \text{ and } \mathrm{ID}_p \text{ is not grouped.} \end{cases} \quad (6)$$

The SIC decoding order is an essential issue in the NOMA-STAR-RIS system, where each user sequentially performs SIC to remove interference in a specific order before decoding its own message. To ensure successful SIC for the considered system, the better $\hat{\mathbf{H}}_{\mathrm{B},b}$ and poorer $\hat{\mathbf{H}}_{\mathrm{B},p}$ cascaded channel condition between ID_b and ID_p at the same STAR-RIS should be determined. Let $\hat{\mathbf{H}}_{\mathrm{B},n} \triangleq \hat{\mathbf{H}}_{\mathrm{B},n}(\mathbf{\Theta}_{\mathsf{R}_k})$ and $\hat{\mathbf{H}}_{\mathrm{B},f} \triangleq \hat{\mathbf{H}}_{\mathrm{B},f}(\mathbf{\Psi}_{\mathsf{R}_k})$. The cascaded channel to determine the SIC order can be expressed as

$$\hat{\mathbf{H}}_{\mathrm{B},b}(\mathsf{X}_{\mathsf{R}_k}) = \begin{cases} \hat{\mathbf{H}}_{\mathrm{B},n}(\mathbf{\Theta}_{\mathsf{R}_k}), & \text{if } \|\hat{\mathbf{H}}_{\mathrm{B},n}\|^2 \geq \|\hat{\mathbf{H}}_{\mathrm{B},f}\|^2, \\ \hat{\mathbf{H}}_{\mathrm{B},f}(\mathbf{\Psi}_{\mathsf{R}_k}), & \text{Otherwise,} \end{cases} \quad (7)$$

$$\hat{\mathbf{H}}_{\mathrm{B},p}(\mathsf{X}_{\mathsf{R}_k}) = \begin{cases} \hat{\mathbf{H}}_{\mathrm{B},f}(\mathbf{\Psi}_{\mathsf{R}_k}), & \text{if } \|\hat{\mathbf{H}}_{\mathrm{B},f}\|^2 \geq \|\hat{\mathbf{H}}_{\mathrm{B},n}\|^2, \\ \hat{\mathbf{H}}_{\mathrm{B},n}(\mathbf{\Theta}_{\mathsf{R}_k}), & \text{Otherwise,} \end{cases} \quad (8)$$

then, the criteria to select the user with better $\mathbf{W}_b$ and poorer $\mathbf{W}_f$ channel conditions can be expressed as

$$\mathbf{W}_b = \begin{cases} \mathbf{W}_n, & \text{if } \|\hat{\mathbf{H}}_{\mathrm{B},b}(\mathsf{X}_{\mathsf{R}_k})\|^2 = \|\hat{\mathbf{H}}_{\mathrm{B},n}(\mathbf{\Theta}_{\mathsf{R}_k})\|^2, \\ \mathbf{W}_f, & \text{if } \|\hat{\mathbf{H}}_{\mathrm{B},b}(\mathsf{X}_{\mathsf{R}_k})\|^2 \neq \|\hat{\mathbf{H}}_{\mathrm{B},n}(\mathbf{\Theta}_{\mathsf{R}_k})\|^2, \end{cases} \quad (9)$$

$$\mathbf{W}_p = \begin{cases} \mathbf{W}_f, & \text{if } \|\hat{\mathbf{H}}_{\mathrm{B},p}(\mathsf{X}_{\mathsf{R}_k})\|^2 = \|\hat{\mathbf{H}}_{\mathrm{B},f}(\mathbf{\Psi}_{\mathsf{R}_k})\|^2, \\ \mathbf{W}_n, & \text{if } \|\hat{\mathbf{H}}_{\mathrm{B},p}(\mathsf{X}_{\mathsf{R}_k})\|^2 \neq \|\hat{\mathbf{H}}_{\mathrm{B},f}(\mathbf{\Psi}_{\mathsf{R}_k})\|^2, \end{cases} \quad (10)$$

where $\mathsf{X}_{\mathsf{R}_k} \in \{\mathbf{\Psi}_{\mathsf{R}_k}, \mathbf{\Theta}_{\mathsf{R}_k}\}$. These expressions compare the channel gains to determine the better and poorer channel conditions, which are crucial for setting the SIC decoding order. Moreover, this approach ensures that the user with the stronger channel condition is decoded later in the SIC process, which is essential for maintaining the integrity of the decoding process and improving overall system performance.

Accordingly, the signal-to-interference-plus-noise ratio (SINR) at ID_b to decode the ID_p's message by applying SIC can be presented as

$$\gamma_b^{\varsigma_p}(\mathbf{W}, \mathsf{X}_{\mathsf{R}_k}, \mathbf{V}) = \frac{|\hat{\mathbf{H}}_{\mathrm{B},b}(\mathsf{X}_{\mathsf{R}_k})\mathbf{W}_p|^2}{\Upsilon_{b,p}(\mathbf{W}, \mathsf{X}_{\mathsf{R}_k}, \mathbf{V})}, \tag{11}$$

where $\Upsilon_{b,p}(\mathbf{W}, \mathsf{X}_{\mathsf{R}_k}, \mathbf{V}) = \sum_{b\in\mathcal{B}} |\hat{\mathbf{H}}_{\mathrm{B},b}(\mathsf{X}_{\mathsf{R}_k})\mathbf{W}_b|^2 + \sum_{p'\in\mathcal{P}\setminus\{p\}} |\hat{\mathbf{H}}_{\mathrm{B},b}(\mathsf{X}_{\mathsf{R}_k})\mathbf{W}_{p'}|^2 + \|\hat{\mathbf{H}}_{\mathrm{B},b}(\mathsf{X}_{\mathsf{R}_k})\mathbf{V}\|^2 + \sigma_b^2$.

To implement the grouping process, ID_b can decode its message from the received signal, in which the SINR including the grouping variable can be expressed as

$$\gamma_b^{\mathrm{AUG}}(\mathbf{W}, \mathsf{X}_{\mathsf{R}_k}, \mathbf{V}, \mathbf{P}) = \frac{|\hat{\mathbf{H}}_{\mathrm{B},b}(\mathsf{X}_{\mathsf{R}_k})\mathbf{W}_b|^2}{\Upsilon_b(\mathbf{W}, \mathsf{X}_{\mathsf{R}_k}, \mathbf{V}, \mathbf{P})}, \tag{12}$$

where $\Upsilon_b(\mathbf{W}, \mathsf{X}_{\mathsf{R}_k}, \mathbf{V}, \mathbf{P}) = \sum_{b'\in\mathcal{B}\setminus\{b\}} |\hat{\mathbf{H}}_{\mathrm{B},b}(\mathsf{X}_{\mathsf{R}_k})\mathbf{W}_{b'}|^2 + \sum_{p'\in\mathcal{P}}(1-[\mathbf{P}]_{bp'})|\hat{\mathbf{H}}_{\mathrm{B},b}(\mathsf{X}_{\mathsf{R}_k})\mathbf{W}_{p'}|^2 + \|\hat{\mathbf{H}}_{\mathrm{B},b}(\mathsf{X}_{\mathsf{R}_k})\mathbf{V}\|^2 + \sigma_b^2$.

Different from ID_b, ID_p can decode its own message directly, in which the SINR can be expressed as

$$\gamma_p^{\varsigma_p}(\mathbf{W}, \mathsf{X}_{\mathsf{R}_k}, \mathbf{V}) = \frac{|\hat{\mathbf{H}}_{\mathrm{B},p}(\mathsf{X}_{\mathsf{R}_k})\mathbf{W}_p|^2}{\Upsilon_p(\mathbf{W}, \mathsf{X}_{\mathsf{R}_k}, \mathbf{V})}, \tag{13}$$

where $\Upsilon_p(\mathbf{W}, \mathsf{X}_{\mathsf{R}_k}, \mathbf{V}) = \sum_{b\in\mathcal{B}} |\hat{\mathbf{H}}_{\mathrm{B},p}(\mathsf{X}_{\mathsf{R}_k})\mathbf{W}_b|^2 + \sum_{p'\in\mathcal{P}\setminus\{p\}} |\hat{\mathbf{H}}_{\mathrm{B},p}(\mathsf{X}_{\mathsf{R}_k})\mathbf{W}_{p'}|^2 + \|\hat{\mathbf{H}}_{\mathrm{B},p}(\mathsf{X}_{\mathsf{R}_k})\mathbf{V}\|^2 + \sigma_p^2$.

According to (11) and (13), the SINR γ_b^{AUG} for ID_b including grouping element $[\mathbf{P}]_{nf}$ can be expressed as

$$\gamma_p^{\mathrm{AUG}}(\mathbf{W}, \mathsf{X}_{\mathsf{R}_k}, \mathbf{V}, \mathbf{P}) = \min_{b\in\mathcal{B}} \left\{ \frac{|\hat{\mathbf{H}}_{\mathrm{B},p}(\mathsf{X}_{\mathsf{R}_k})\mathbf{W}_p|^2}{\Upsilon_p(\mathbf{W}, \mathsf{X}_{\mathsf{R}_k}, \mathbf{V})}, \frac{|\hat{\mathbf{H}}_{\mathrm{B},b}(\mathsf{X}_{\mathsf{R}_k})\mathbf{W}_p|^2}{[\mathbf{P}]_{nf}\Upsilon_{b,p}(\mathbf{W}, \mathsf{X}_{\mathsf{R}_k}, \mathbf{V})} \right\}, \tag{14}$$

In (14), when two users are not in a group (i.e. $[\mathbf{P}]_{nf} = 0$), the right-hand side (RHS) inside the min operator will go to infinity. Thus, by using (12) ID_p only decodes its own message. By doing so, the proposed scheme is now switched to the conventional one using conventional beamforming assisted by the STAR-RIS without NOMA, which will be discussed in Remark 1.

Remark 1. Based on SINRs of ID_b and ID_p in (12) and (14), respectively, the AUG scheme can be applied. When $[\mathbf{P}]_{nf} = 1$, two users with different zones are grouped as done in [34], while $[\mathbf{P}]_{nf} = 0$, these users are not in the group or it can be said the BS serves users directly through the assistance of multiple STAR-RIS as done in [10]. Therefore, the strategy of the proposed AUG scheme can be switched from a grouping scheme to the not grouping scheme by flexibly adjusting the user grouping element $[\mathbf{P}]_{nf} = 1$ and $[\mathbf{P}]_{nf} = 0$, respectively.

Considering SPC, a packet of d information bits at the BS is transmitted to ID_b and ID_p over blocklength (number of channel uses) A, with $A > 100$ [36], the capacity at ID_b and ID_p can be approximated, respectively, as

$$R_b(\mathbf{W}, \mathsf{X}_{\mathsf{R}_k}, \mathbf{V}, \mathbf{P}) = A\big[C(\gamma_b^{\mathrm{AUG}}(\mathbf{W}, \mathsf{X}_{\mathsf{R}_k}, \mathbf{V}, \mathbf{P})) - \sqrt{\upsilon(\gamma_b^{\mathrm{AUG}}(\mathbf{W}, \mathsf{X}_{\mathsf{R}_k}, \mathbf{V}, \mathbf{P}))/A}\big]Q^{-1}(\varpi_b), \tag{15}$$

$$R_p(\mathbf{W}, \mathsf{X}, \mathbf{V}, \mathbf{P}) = A\big[C(\gamma_p^{\mathrm{AUG}}(\mathbf{W}, \mathsf{X}_{\mathsf{R}_k}, \mathbf{V}, \mathbf{P})) - \sqrt{\upsilon(\gamma_p^{\mathrm{AUG}}(\mathbf{W}, \mathsf{X}_{\mathsf{R}_k}, \mathbf{V}, \mathbf{P}))/A}\big]Q^{-1}(\varpi_p), \tag{16}$$

where ϖ_u with $u \in \{b, p\}$ is instantaneous BLER at ID_b and ID_p, $Q^{-1}(.)$ is the inverse Gaussian Q-function, $\upsilon(x) \triangleq (1 - (1+x)^{-2})(\log_2 e)^2$ and $C(x) \triangleq \ln(1+x)$ denote the channel dispersion and the Shannon capacity with $x \in \{\gamma_b^{\mathrm{AUG}}, \gamma_p^{\mathrm{AUG}}\}$, respectively.

D. Spectral Efficiency Maximization

Our main goal is to maximize the spectral efficiency of the proposed AUG scheme subject to EH constraints for energy users, maximum power budget at BS, the phase shift of reflection and transmission constraints at STAR-RIS by joint design of linear precoding matrix $\mathbf{W}$, the phase shift of reflection $\mathbf{\Theta}_{\mathsf{R}_k}$ and transmission $\mathbf{\Psi}_{\mathsf{R}_k}$, energy beamforming matrix $\mathbf{V}$, and user grouping $\mathbf{P}$ which can be formulated as

$$\max_{\substack{\mathbf{W},\mathbf{\Theta}_{\mathsf{R}_k},\\ \mathbf{\Psi}_{\mathsf{R}_k},\mathbf{V},\mathbf{P}}} \mathcal{R}_{\sum} \triangleq \sum_{b\in\mathcal{B}} R_b(\mathbf{W}, \mathsf{X}_{\mathsf{R}_k}, \mathbf{V}, \mathbf{P}) + \sum_{p\in\mathcal{P}} R_p(\mathbf{W}, \mathsf{X}_{\mathsf{R}_k}, \mathbf{V}, \mathbf{P}) \tag{17a}$$

$$\mathrm{E}_q(\mathbf{V}, \mathbf{W}) \geq \bar{\mathrm{E}}_q, \quad \forall q \in \mathcal{Q}, \tag{17b}$$

$$\|\mathbf{W}_n\|^2 + \|\mathbf{W}_f\|^2 + \|\mathbf{V}\|^2 \leq \bar{P}_{\mathrm{BS}}, \tag{17c}$$

$$[\mathbf{P}]_{nf} \in \{0, 1\}, \quad \forall n \in \mathcal{N}, \forall f \in \mathcal{F}, \tag{17d}$$

$$\sum_{n\in\mathcal{N}} [\mathbf{P}]_{nf} \leq 1, \sum_{f\in\mathcal{F}} [\mathbf{P}]_{nf} \leq 1, \tag{17e}$$

$$\varpi_b \leq \bar{\varpi}_b, \ \varpi_p \leq \bar{\varpi}_p, \tag{17f}$$

$$\theta_{k,l_r} = \left\{0, \frac{\theta_{k,l_r} 2\pi}{\mathsf{Res}_k}, \cdots, \frac{(\mathsf{Res}_k - 1)\theta_{k,l_r} 2\pi}{\mathsf{Res}_k}\right\}, \tag{17g}$$

$$\psi_{k,l_t} = \left\{0, \frac{\psi_{k,l_t} 2\pi}{\mathsf{Res}_k}, \cdots, \frac{(\mathsf{Res}_k - 1)\psi_{k,l_t} 2\pi}{\mathsf{Res}_k}\right\}, \tag{17h}$$

where constraint (17b) indicates that the harvested energy for E_q is greater than the predetermined threshold $\bar{\mathrm{E}}_q$. Constraint (17c) indicates that the total power of all users must be less than equal maximum power budget of the BS. Constraints (17d) and (17e) indicate the user grouping criteria for information users. Constraint (17f) indicates that the instantaneous BLER must be less than the threshold BLER. The constraints (17g) and (17h) indicate the phase shift of reflection and transmission of all STAR-RIS that have discrete values. It is clear that the problem formulation (17) is non-convex subject to mixed integer constraints, which is a non-convex problem belonging to the mixed integer non-convex programming class.

III. The Proposed SEM Algorithm

To tackle problem (17), the standard way to overcome the binary property is by relaxing the binary and discrete variables into continuous ones. The relaxed form of the original problem (17) can be expressed as

$$\max_{\substack{\mathbf{W},\mathbf{\Theta}_{\mathsf{R}_k},\\ \mathbf{\Psi}_{\mathsf{R}_k},\mathbf{V},\mathbf{P}}} \mathcal{R}_{\sum} \triangleq \sum_{b\in\mathcal{B}} R_b(\mathbf{W}, \mathsf{X}_{\mathsf{R}_k}, \mathbf{V}, \mathbf{P}) + \sum_{p\in\mathcal{P}} R_p(\mathbf{W}, \mathsf{X}_{\mathsf{R}_k}, \mathbf{V}, \mathbf{P}) \tag{18a}$$

$$\text{s.t. } [\mathbf{P}]_{nf} \in [0, 1], \forall n \in \mathcal{N}, \forall f \in \mathcal{F}, \tag{18b}$$

$$\theta_{k,l_r} \in [0, 2\pi], \forall k \in K, \ l_r \in L_r, \tag{18c}$$

$$\psi_{k,l_t} \in [0, 2\pi], \forall k \in K, \ l_t \in L_t, \tag{18d}$$

$$(17b), \ (17c), \ (17e), \ (17f). \tag{18e}$$

We introduce auxiliary variables $\mathbf{r} \in \{r_b, r_p\}_{b\in\mathcal{B},\ p\in\mathcal{P}}$ with $\mathbf{r} > 0$ representing as soft data rates, $\boldsymbol{\zeta} \in \{\zeta_b, \zeta_p\}_{b\in\mathcal{B},\ p\in\mathcal{P}}$ as SINRs of ID_b and ID_p, $\bar{\mathsf{R}}_b$ and $\bar{\mathsf{R}}_p$ as minimum data rates

thresholds for ID_b and ID_p, respectively. Thus, (18) can be re-expressed as

$$\max_{\substack{\mathbf{W},\mathbf{V},\mathbf{P},\mathbf{r},\\ \boldsymbol{\Theta}_{\mathsf{R}_k},\boldsymbol{\Psi}_{\mathsf{R}_k},\boldsymbol{\zeta}}} \bar{\mathcal{R}}_{\sum} \triangleq \sum_{b\in\mathcal{B}} r_b + \sum_{p\in\mathcal{P}} r_p \tag{19a}$$

$$\text{s.t. } A\big[C(\gamma_b^{\mathrm{AUG}}(\mathbf{W},\mathsf{X}_{\mathsf{R}_k},\mathbf{V},\mathbf{P})) - \sqrt{\upsilon(\gamma_b^{\mathrm{AUG}}(\mathbf{W},\mathsf{X}_{\mathsf{R}_k},\mathbf{V},\mathbf{P}))/A}\big]Q^{-1}(\varpi_b) \geq r_b, \tag{19b}$$

$$A\big[C(\gamma_p^{\mathrm{AUG}}(\mathbf{W},\mathsf{X}_{\mathsf{R}_k},\mathbf{V},\mathbf{P})) - \sqrt{\upsilon(\gamma_p^{\mathrm{AUG}}(\mathbf{W},\mathsf{X}_{\mathsf{R}_k},\mathbf{V},\mathbf{P}))/A}\big]Q^{-1}(\varpi_p) \geq r_p, \tag{19c}$$

$$\gamma_b^{\mathrm{AUG}}(\mathbf{W},\mathsf{X}_{\mathsf{R}_k},\mathbf{V},\mathbf{P}) \geq \zeta_b^{-1}, \tag{19d}$$

$$\gamma_p^{\mathrm{AUG}}(\mathbf{W},\mathsf{X}_{\mathsf{R}_k},\mathbf{V},\mathbf{P}) \geq \zeta_p^{-1}, \tag{19e}$$

$$\ln(1+\zeta_b^{-1}) \geq \bar{\mathsf{R}}_b, \tag{19f}$$

$$\ln(1+\zeta_p^{-1}) \geq \bar{\mathsf{R}}_p, \tag{19g}$$

$$(17b), (17c), (17e), (17f), (18b), (18c), (18d). \tag{19h}$$

The formulated problem in (19) is non-convex and fractional form. To tackle this problem efficiently, we decouple problem (19) into phase shift optimization and beamforming optimization subproblems and then solve them alternatively [37]. The phase shift optimization consists of phase shift of reflection $\boldsymbol{\Theta}_{\mathsf{R}_k}$ and transmission $\boldsymbol{\Psi}_{\mathsf{R}_k}$ of the STAR-RIS while the beamforming optimization consists of linear precoding matrix $\mathbf{W}$, energy beamforming matrix $\mathbf{V}$, and user grouping $\mathbf{P}$. First, we tackle the phase shift optimization with the fixed beamforming optimization variables ($\mathbf{W}$, $\mathbf{V}$, $\mathbf{P}$). Then, relying on the optimized phase shift of reflection $\boldsymbol{\Theta}_{\mathsf{R}_k}$ and transmission $\boldsymbol{\Psi}_{\mathsf{R}_k}$ of the STAR-RIS, we propose an iterative algorithm to achieve the beamforming optimization variables. We solve this subproblem until convergence to solve the problem (19) efficiently.

A. Phase Shift Optimization

Now, we start to find the optimal solution of phase shift of reflection $\boldsymbol{\Theta}_{\mathsf{R}_k}$ and transmission $\boldsymbol{\Psi}_{\mathsf{R}_k}$ of the STAR-RIS. By fixing the beamforming optimization variables ($\mathbf{W}$, $\mathbf{V}$, $\mathbf{P}$), problem (19) can be rewritten as

$$\max_{\boldsymbol{\Theta}_{\mathsf{R}_k},\boldsymbol{\Psi}_{\mathsf{R}_k}} \bar{\mathcal{R}}_{\sum} \triangleq \sum_{b\in\mathcal{B}} r_b + \sum_{p\in\mathcal{P}} r_p \tag{20a}$$

$$\text{s.t. } (18c), (18d). \tag{20b}$$

Note that the objective function (20a) is a concave problem while the constraints (18c) and (18d) are linear constraints. However, when solving problem (20), the optimal solutions of $\psi_{k,l}^{(i)}$ and $\theta_{k,l}^{(i)}$ still have continuous values. To address this problem, we apply the rounding function after obtaining the optimal solution to the problem (20) as

$$\mathsf{Y}^{\star} = \lceil \mathsf{Y}^{(i)} - \alpha \rceil,\ \mathsf{Y}^{(i)} \in \boldsymbol{\Theta}_{\mathsf{R}_k}^{(i)}, \boldsymbol{\Psi}_{\mathsf{R}_k}^{(i)},\ k \in \mathcal{K}, \tag{21}$$

where $\mathsf{Y}^{\star}$ denotes the rounded value of $\mathsf{Y}^{(i)}$ and α denotes the range of the rounding function. To tackle this problem directly, we introduce the Algorithm 1 based on the bisection search algorithm to approximate the concave problem (20) efficiently including the rounding function.

Algorithm 1 Bisection Search to Solving Problem (20)

Input: b, p.
Output: $\boldsymbol{\Psi}_{\mathsf{R}_k}^{\star}$, $\boldsymbol{\Theta}_{\mathsf{R}_k}^{\star}$.

```
for k = 1, 2, 3 ··· K do
    Initialization :
    Lower bound p_{l,t}^L and p_{l,r}^L, upper bound p_{l,t}^U and p_{l,r}^U, and α = 0.7;
    for l = 1, 2, 3 ··· L do
        Calculate p_t = (p_{l,t}^L + p_{l,t}^U)/2; p_r = (p_{l,r}^L + p_{l,r}^U)/2;
        Update ψ_{k,l}(p_t) and θ_{k,l}(p_r);
        Solve the problem (20);
        Update new p_{l,t}^L, p_{l,r}^L, p_{l,t}^U and p_{l,r}^U;
    end for
end for
if Convergence then
    Rounded up (Θ_{R_k}, Ψ_{R_k}) based on (21);
    Θ*_{R_k} ← Θ_{R_k}; Ψ*_{R_k} ← Ψ_{R_k};
end if
```

B. Beamforming Optimization

In this section, we focus on beamforming optimization. Given by phase shift reflection $\boldsymbol{\Theta}$ and transmission $\boldsymbol{\Psi}$ at STAR-RIS obtained from the phase shift optimization, the problem in (19) can be rewritten as

$$\max_{\mathbf{W},\mathbf{V},\mathbf{P},\mathbf{r},\boldsymbol{\zeta}} \bar{\mathcal{R}}_{\sum} \triangleq \sum_{b\in\mathcal{B}} r_b + \sum_{p\in\mathcal{P}} r_p \tag{22a}$$

$$\text{s.t. } (17b),\ (17c),\ (17e),\ (17f),\ (18b),\ (19b),\ (19c),\ (19d),\ (19e),\ (19f),\ (19g). \tag{22b}$$

It should be noted that the objective function (22) is concave while constraints (17b), (19b)-(19g) are non-convex.

The following Lemmas are described to make constraints (17b), (19d), and (19e) convex, with x and y indicating the initial point of x and y, respectively, while $\bar{x}$ and $\bar{y}$ indicate feasible points of x and y in every iteration, respectively.

Lemma 1. $\forall x \in \mathbb{C}, \forall y \in \mathbb{R}, 0 < y$, it is true that

$$x^2 y^{-1} \geq 2\bar{x}^* x \bar{y}^{-1} - |\bar{x}|^2 y \bar{y}^{-2}. \tag{23}$$

Proof. See Appendix A of [38] to proof of Lemma 1. □

Lemma 2. $\forall y \in \mathbb{R}^2, \forall x \in \mathbb{R}^2$ it is true that

$$(xy)^{-1} \leq (\bar{x}^2 y^2 + x^2 \bar{y}^2)(2x^2 \bar{x} y^2 \bar{y})^{-1}. \tag{24}$$

Proof. The proof of Lemma 2 has been explained in [39]. The left-hand-side (LHS) $(xy)^{-1}$ indicates that the lower bound, and the right-hand side (RHS) of (24) is convex based on the IA method. □

We are now in the position to address constraint (17b). We first transform it into an equivalent expression as

$$\mathrm{E}_q(\mathbf{V},\mathbf{W}) \geq b_q - a_q^{-1} \ln\left(\frac{\bar{P}_q(1-\Omega_q)^{-1}}{\bar{\mathrm{E}}_q + \bar{P}_q\Omega_q/(1-\Omega_q)} - 1\right) \triangleq \eta_q. \tag{25}$$

It should be noted that the LHS in (25) is convex. In the iterative algorithm, let us introduce $x^{(i)}$ as the feasible point

of x at the i-th iteration. Then, to approximate it around the point $(\mathbf{V}^{(i)},\mathbf{W}^{(i)})$, we can utilize Lemma 1 as follows:

$$\begin{aligned}
&\mathrm{E}_q(\mathbf{V},\mathbf{W})\\
&\geq 2\Re\big\{\mathbf{h}_{\mathrm{BS},\mathrm{E}_q}\mathrm{Trace}\big((\mathbf{V}^{(i)})^H\mathbf{h}^H_{\mathrm{BS},\mathrm{E}_q}\mathbf{V}\big)\big\}-\|\mathbf{h}^H_{\mathrm{BS},\mathrm{E}_q}\mathbf{V}^{(i)}\|^2\\
&+\sum_{n\in\mathcal{N}}\left[2\Re\big\{\mathbf{h}_{\mathrm{BS},\mathrm{E}_q}(\mathbf{W}_n^{(i)})^H\mathbf{h}^H_{\mathrm{BS},\mathrm{E}_q}\mathbf{W}_b\big\}-|\mathbf{h}^H_{\mathrm{BS},\mathrm{E}_q}\mathbf{W}_n^{(i)}|^2\right]\\
&+\sum_{f\in\mathcal{F}}\left[2\Re\big\{\mathbf{h}_{\mathrm{BS},\mathrm{E}_q}(\mathbf{W}_f^{(i)})^H\mathbf{h}^H_{\mathrm{BS},\mathrm{E}_q}\mathbf{W}_p\big\}-|\mathbf{h}^H_{\mathrm{BS},\mathrm{E}_q}\mathbf{W}_f^{(i)}|^2\right]\\
&\triangleq \mathrm{E}_q^{(i)}(\mathbf{V},\mathbf{W}). \qquad (26)
\end{aligned}$$

Following convex approximation, (17b) can be iteratively approximated as

$$\mathrm{E}_q^{(i)}(\mathbf{V},\mathbf{W}) \quad \geq \eta_q, \forall q\in\mathcal{Q}. \qquad (27)$$

For constraint (19b), let $\hat{f}_b(\mathbf{W},\mathsf{X}_{\mathsf{R}_k},\mathbf{V},\mathbf{P}) \triangleq \ln(1+\gamma_b^{\mathrm{AUG}}(\mathbf{W},\mathsf{X}_{\mathsf{R}_k},\mathbf{V},\mathbf{P}))$, $\xi_b \triangleq Q^{-1}(\varpi_b)/\sqrt{A}$ and $g_b(\mathbf{W},\mathsf{X}_{\mathsf{R}_k},\mathbf{V},\mathbf{P}) \triangleq \sqrt{1-1/(1+\gamma_b^{\mathrm{AUG}}(\mathbf{W},\mathsf{X}_{\mathsf{R}_k},\mathbf{V},\mathbf{P}))^2}$. Then, (15) can be re-expressed as

$$\begin{aligned}
&r_b(\mathbf{W},\mathsf{X}_{\mathsf{R}_k},\mathbf{V},\mathbf{P})\\
&\quad=A\Big[\hat{f}_b(\mathbf{W},\mathsf{X}_{\mathsf{R}_k},\mathbf{V},\mathbf{P})-\xi_b g_b(\mathbf{W},\mathsf{X}_{\mathsf{R}_k},\mathbf{V},\mathbf{P})\Big]. \qquad (28)
\end{aligned}$$

By following (78) in [32, (78)], the lower bounding concave function for $\hat{f}_b$ can be approximated as

$$\begin{aligned}
\hat{f}_b(\mathbf{W},\mathsf{X}_{\mathsf{R}_k},\mathbf{V},\mathbf{P}) &\geq \bar{a}_b^{(i)}-|\hat{\mathbf{H}}_{\mathrm{B},b}(\mathsf{X}_{\mathsf{R}_k})\mathbf{W}_b^{(i)}|^2(2\Re\{\Xi_b^{(i)}\})^{-1}\\
&\quad-\bar{b}_b^{(i)}|\hat{\mathbf{H}}_{\mathrm{B},b}(\mathsf{X}_{\mathsf{R}_k})\mathbf{W}_b|^2-\bar{c}_b^{(i)}\Upsilon_b(\mathbf{W},\mathsf{X}_{\mathsf{R}_k},\mathbf{V},\mathbf{P})\\
&\triangleq \hat{f}_b^{(i)}(\mathbf{W},\mathsf{X}_{\mathsf{R}_k},\mathbf{V},\mathbf{P}). \qquad (29)
\end{aligned}$$

Under the trust region constraint by

$$2\Re\{\Xi_b^{(i)}\}>0, \qquad (30)$$

where

$$\bar{a}_b^{(i)}=\hat{f}_b(\mathbf{W}^{(i)},\mathsf{X}_{\mathsf{R}_k},\mathbf{V},\mathbf{P})+2-\frac{|\hat{\mathbf{H}}_{\mathrm{B},b}(\mathsf{X}_{\mathsf{R}_k})\mathbf{W}_b^{(i)}|^2\sigma_b^2}{d_b^{(i)}e_b^{(i)}}, \qquad (31)$$

$$\Xi_b^{(i)}=\mathbf{W}_b^{(i)}(\mathsf{X}_{\mathsf{R}_k})\hat{\mathbf{H}}_{\mathrm{B},b}\hat{\mathbf{H}}_{\mathrm{B},b}(\mathsf{X}_{\mathsf{R}_k})\mathbf{W}_b-|\hat{\mathbf{H}}_{\mathrm{B},b}(\mathsf{X}_{\mathsf{R}_k})\mathbf{W}_b^{(i)}|^2, \qquad (32)$$

$$0<\bar{b}_b^{(i)}=e_b^{(i)}(d_b^{(i)}|\hat{\mathbf{H}}_{\mathrm{B},b}(\mathsf{X}_{\mathsf{R}_k})\mathbf{W}_b^{(i)}|^2)^{-1}, \qquad (33)$$

$$0<\bar{c}_b^{(i)}=|\hat{\mathbf{H}}_{\mathrm{B},b}(\mathsf{X}_{\mathsf{R}_k})\mathbf{W}_b^{(i)}|^2(d_b^{(i)}e_b^{(i)})^{-1}, \qquad (34)$$

$$d_b^{(i)}\triangleq|\hat{\mathbf{H}}_{\mathrm{B},b}(\mathsf{X}_{\mathsf{R}_k})\mathbf{W}_b^{(i)}|^2+\sigma_b^2, \qquad (35)$$

$$\begin{aligned}
e_b^{(i)}\triangleq&\sum_{b'\in\mathcal{B}\setminus\{b\}}|\hat{\mathbf{H}}_{\mathrm{B},b}(\mathsf{X}_{\mathsf{R}_k})\mathbf{W}_{b'}^{(i)}|^2+\sum_{p'\in\mathcal{P}}(1-[\mathbf{P}]_{bp'})\\
&\times|\hat{\mathbf{H}}_{\mathrm{B},b}(\mathsf{X}_{\mathsf{R}_k})\mathbf{W}_{p'}^{(i)}|^2+\|\hat{\mathbf{H}}_{\mathrm{B},b}(\mathsf{X}_{\mathsf{R}_k})\mathbf{V}\|^2+\sigma_b^2. \qquad (36)
\end{aligned}$$

Thus, the function $\hat{f}_b^{(i)}$ in (29) is concave over the trust region in (30) and it matches with $\hat{f}_b(\mathbf{W},\mathsf{X}_{\mathsf{R}_k},\mathbf{V},\mathbf{P})$ at $\mathbf{W}^{(i)}$:

$$\hat{f}_b^{(i)}(\mathbf{W}^{(i)},\mathsf{X}_{\mathsf{R}_k},\mathbf{V},\mathbf{P})=\hat{f}_b(\mathbf{W}^{(i)},\mathsf{X}_{\mathsf{R}_k},\mathbf{V},\mathbf{P}). \qquad (37)$$

And, $g_b(\mathbf{W},\mathsf{X}_{\mathsf{R}_k},\mathbf{V},\mathbf{P})$ by following (81) in [32, (81)] can be upper bounding convex function as

$$g_b(\mathbf{W},\mathsf{X}_{\mathsf{R}_k},\mathbf{V},\mathbf{P})=j_b^{(i)}-k_b^{(i)}\frac{(\Upsilon_b(\mathbf{W},\mathsf{X}_{\mathsf{R}_k},\mathbf{V},\mathbf{P}))^2}{(|\hat{\mathbf{H}}_{\mathrm{B},b}(\mathsf{X}_{\mathsf{R}_k})\mathbf{W}_b|^2+\sigma_b^2)^2}, \qquad (38)$$

where

$$\begin{aligned}
0<j_b^{(i)}=&\sqrt{1-1/(1+\gamma_b^{\mathrm{AUG}}(\mathbf{W}^{(i)},\mathsf{X}_{\mathsf{R}_k},\mathbf{V},\mathbf{P}))^2}/2\\
&+1/2\sqrt{1-1/(1+\gamma_b^{\mathrm{AUG}}(\mathbf{W}^{(i)},\mathsf{X}_{\mathsf{R}_k},\mathbf{V},\mathbf{P}))^2}, \qquad (39)\\
0<k_b^{(i)}=&1/2\sqrt{1-1/(1+\gamma_b^{\mathrm{AUG},2}(\mathbf{W}^{(i)},\mathsf{X}_{\mathsf{R}_k},\mathbf{V},\mathbf{P}))^2}. \qquad (40)
\end{aligned}$$

The RHS term in (38) is still a non-convex function. By following Appendix C in [32, Appendix C], we can approximate the lower bound of the RHS in (38) as

$$\begin{aligned}
\frac{(\Upsilon_b(\mathbf{W},\mathsf{X}_{\mathsf{R}_k},\mathbf{V},\mathbf{P}))^2}{(|\hat{\mathbf{H}}_{\mathrm{B},b}(\mathsf{X}_{\mathsf{R}_k})\mathbf{W}_b|^2+\sigma_b^2)^2}&\geq\frac{4e_b^{(i)}}{(d_b^{(i)})^2}\Omega_b-\frac{2(e_b^{(i)})^2}{(d_b^{(i)})^3}\\
&\times\big(|\hat{\mathbf{H}}_{\mathrm{B},b}(\mathsf{X}_{\mathsf{R}_k})\mathbf{W}_b|^2+\sigma_b^2\big)-(\Upsilon_b(\mathbf{W},\mathsf{X}_{\mathsf{R}_k},\mathbf{V},\mathbf{P}))^2/(d_b^2)^2, \qquad (41)
\end{aligned}$$

where $\Omega_b=\sum_{b'\in\mathcal{B}\setminus\{b\}}\big(2\Re\{(\hat{\mathbf{H}}_{\mathrm{B},b}(\mathsf{X}_{\mathsf{R}_k})\mathbf{W}_{b'}^{(i)})^*\hat{\mathbf{H}}_{\mathrm{B},b}(\mathsf{X}_{\mathsf{R}_k})\mathbf{W}_{b'}\}-|\hat{\mathbf{H}}_{\mathrm{B},b}(\mathsf{X}_{\mathsf{R}_k})\mathbf{W}_{b'}^{(i)}|^2\big)+\sum_{p'\in\mathcal{P}}\big(2\Re\{((1-[\mathbf{P}]_{bp'})\times\hat{\mathbf{H}}_{\mathrm{B},b}(\mathsf{X}_{\mathsf{R}_k})\mathbf{W}_{p'}^{(i)})^*((1-[\mathbf{P}]_{bp'})\hat{\mathbf{H}}_{\mathrm{B},b}(\mathsf{X}_{\mathsf{R}_k})\mathbf{W}_{p'})\}-(1-[\mathbf{P}]_{bp'})|\hat{\mathbf{H}}_{\mathrm{B},b}(\mathsf{X}_{\mathsf{R}_k})\mathbf{W}_{p'}^{(i)}|^2\big)+\|\hat{\mathbf{H}}_{\mathrm{B},b}(\mathsf{X}_{\mathsf{R}_k})\mathbf{V}\|^2+\sigma_b^2$, under the trust region constrained by

$$|\hat{\mathbf{H}}_{\mathrm{B},b}(\mathsf{X}_{\mathsf{R}_k})\mathbf{W}_b|^2+\sigma_b^2\leq 2d_b^{(i)}, \qquad (42a)$$

$$\frac{1}{d_b^{(i)}}\Big(|\hat{\mathbf{H}}_{\mathrm{B},b}(\mathsf{X}_{\mathsf{R}_k})\mathbf{W}_b|^2+\sigma_b^2\Big)\leq\frac{2}{e_b^{(i)}}\Omega_b. \qquad (42b)$$

By plugging (41) into (38), we have

$$\begin{aligned}
g_b(\mathbf{W},\mathsf{X}_{\mathsf{R}_k},\mathbf{V},\mathbf{P})&\leq j_b^{(i)}-\frac{4e_b^{(i)}k_b^{(i)}}{(d_b^{(i)})^2}\Omega_b+\frac{2(e_b^{(i)})^2k_b^{(i)}}{(d_b^{(i)})^3}\\
&\times\Big(|\hat{\mathbf{H}}_{\mathrm{B},b}(\mathsf{X}_{\mathsf{R}_k})\mathbf{W}_b|^2+\sigma_b^2\Big)+\frac{\big(\Upsilon_b(\mathbf{W},\mathsf{X}_{\mathsf{R}_k},\mathbf{V},\mathbf{P})\big)^2k_b^{(i)}}{(d_b^{(i)})^2}\\
&\triangleq g_b^{(i)}((\mathbf{W},\mathsf{X}_{\mathsf{R}_k},\mathbf{V},\mathbf{P})). \qquad (43)
\end{aligned}$$

From (29) and (43), the (28) iteratively can be re-expressed as

$$\begin{aligned}
r_b(\mathbf{W},\mathsf{X}_{\mathsf{R}_k},\mathbf{V},\mathbf{P})&\geq A\big[\hat{f}_b^{(i)}(\mathbf{W},\mathsf{X}_{\mathsf{R}_k},\mathbf{V},\mathbf{P})\\
&\quad-\xi_b g_b^{(i)}(\mathbf{W},\mathsf{X}_{\mathsf{R}_k},\mathbf{V},\mathbf{P})\big]\triangleq r_b^{(i)}(\mathbf{W},\mathsf{X}_{\mathsf{R}_k},\mathbf{V},\mathbf{P}). \qquad (44)
\end{aligned}$$

For constraint (19c), let $\hat{f}_p(\mathbf{W},\mathsf{X}_{\mathsf{R}_k},\mathbf{V}) \triangleq \ln(1+\gamma_p^{\varsigma_p}(\mathbf{W},\mathsf{X}_{\mathsf{R}_k},\mathbf{V}))$, $\hat{f}_{b,p}(\mathbf{W},\mathsf{X}_{\mathsf{R}_k},\mathbf{V},\mathbf{P}) \triangleq \ln(1+(|\hat{\mathbf{H}}_{\mathrm{B},b}(\mathsf{X}_{\mathsf{R}_k})\mathbf{W}_p|^2)/([\mathbf{P}]_{nf}\Upsilon_{b,p}(\mathbf{W},\mathsf{X}_{\mathsf{R}_k},\mathbf{V})))$, $g_p(\mathbf{W},\mathsf{X}_{\mathsf{R}_k},\mathbf{V}) \triangleq \sqrt{1-1/(1+\gamma_p^{\varsigma_p}(\mathbf{W},\mathsf{X}_{\mathsf{R}_k},\mathbf{V}))^2}$, $\xi_p \triangleq Q^{-1}(\varpi_p)/\sqrt{A}$, $g_{b,p}(\mathbf{W},\mathsf{X}_{\mathsf{R}_k},\mathbf{V},\mathbf{P}) \triangleq \sqrt{1-1/(1+(|\hat{\mathbf{H}}_{\mathrm{B},b}(\mathsf{X}_{\mathsf{R}_k})\mathbf{W}_p|^2/([\mathbf{P}]_{nf}\Upsilon_{b,p}(\mathbf{W},\mathsf{X}_{\mathsf{R}_k},\mathbf{V})))^2}$. Without loss generality, we can re-express constraint (19c) from (14) as

$$r_p(\mathbf{W},\mathsf{X}_{\mathsf{R}_k},\mathbf{V})=A\left[\hat{f}_p(\mathbf{W},\mathsf{X}_{\mathsf{R}_k},\mathbf{V})-\xi_p g_p(\mathbf{W},\mathsf{X}_{\mathsf{R}_k},\mathbf{V})\right], \qquad (45a)$$

$$\begin{aligned}
&r_p(\mathbf{W},\mathsf{X}_{\mathsf{R}_k},\mathbf{V},\mathbf{P})\\
&=A\left[\hat{f}_{b,p}(\mathbf{W},\mathsf{X}_{\mathsf{R}_k},\mathbf{V},\mathbf{P})-\xi_p g_{b,p}(\mathbf{W},\mathsf{X}_{\mathsf{R}_k},\mathbf{V},\mathbf{P})\right], \qquad (45b)
\end{aligned}$$

Then, similar to (28), by following (78) in [32, (78)], the lower bounding concave function for $\hat{f}_p$ in (45a) can be approximated as

$$\begin{aligned}
\hat{f}_p(\mathbf{W},\mathsf{X}_{\mathsf{R}_k},\mathbf{V})&\geq\bar{a}_p^{(i)}-|\hat{\mathbf{H}}_{\mathrm{B},p}(\mathsf{X}_{\mathsf{R}_k})\mathbf{W}_p^{(i)}|^2(2\Re\{\Xi_p^{(i)}\})^{-1}\\
&\quad-\bar{b}_p^{(i)}|\hat{\mathbf{H}}_{\mathrm{B},p}(\mathsf{X}_{\mathsf{R}_k})\mathbf{W}_p|^2-\bar{c}_p^{(i)}\Upsilon_p(\mathbf{W},\mathsf{X}_{\mathsf{R}_k},\mathbf{V})\\
&\triangleq\hat{f}_p^{(i)}(\mathbf{W},\mathsf{X}_{\mathsf{R}_k},\mathbf{V}). \qquad (46)
\end{aligned}$$

Under the trust region constraint by

$$2\Re\{\Xi_p^{(i)}\} > 0, \tag{47}$$

where

$$\bar{a}_p^{(i)} = \hat{f}_p(\mathbf{W}^{(i)}, \mathsf{X}_{\mathsf{R}_k}, \mathbf{V}) + 2 - \frac{|\hat{\mathbf{H}}_{\mathrm{B},p}(\mathsf{X}_{\mathsf{R}_k})\mathbf{W}_p^{(i)}|^2\sigma_p^2}{d_p^{(i)}e_p^{(i)}}, \tag{48}$$

$$\Xi_p^{(i)} = (\mathbf{W}_p^{(i)})(\mathsf{X}_{\mathsf{R}_k})\hat{\mathbf{H}}_{\mathrm{B},p}\hat{\mathbf{H}}_{\mathrm{B},p}(\mathsf{X}_{\mathsf{R}_k})\mathbf{W}_p - |\hat{\mathbf{H}}_{\mathrm{B},p}(\mathsf{X}_{\mathsf{R}_k})\mathbf{W}_p^{(i)}|^2, \tag{49}$$

$$0 < \bar{b}_p^{(i)} = e_p^{(i)}(d_p^{(i)}|\hat{\mathbf{H}}_{\mathrm{B},p}(\mathsf{X}_{\mathsf{R}_k})\mathbf{W}_p^{(i)}|^2)^{-1}, \tag{50}$$

$$0 < \bar{c}_p^{(i)} = |\hat{\mathbf{H}}_{\mathrm{B},p}(\mathsf{X}_{\mathsf{R}_k})\mathbf{W}_p^{(i)}|^2(d_p^{(i)}e_p^{(i)})^{-1}, \tag{51}$$

$$d_p^{(i)} \triangleq |\hat{\mathbf{H}}_{\mathrm{B},p}(\mathsf{X}_{\mathsf{R}_k})\mathbf{W}_p^{(i)}|^2 + \sigma_p^2, \tag{52}$$

$$e_p^{(i)} \triangleq \sum_{b\in\mathcal{B}} |\hat{\mathbf{H}}_{\mathrm{B},p}(\mathsf{X}_{\mathsf{R}_k})\mathbf{W}_b|^2 + \sum_{p'\in\mathcal{P}\setminus\{p\}} |\hat{\mathbf{H}}_{\mathrm{B},p}(\mathsf{X}_{\mathsf{R}_k})\mathbf{W}_{p'}|^2 + \|\hat{\mathbf{H}}_{\mathrm{B},p}(\mathsf{X}_{\mathsf{R}_k})\mathbf{V}\|^2 + \sigma_p^2. \tag{53}$$

Thus, the function $\hat{f}_p^{(i)}$ in (45a) is concave over the trust region in (47) and it matches with $\hat{f}_p(\mathbf{W}, \mathsf{X}_{\mathsf{R}_k}, \mathbf{V})$ at $\mathbf{W}^{(i)}$:

$$\hat{f}_p^{(i)}(\mathbf{W}^{(i)}, \mathsf{X}_{\mathsf{R}_k}, \mathbf{V}) = \hat{f}_p(\mathbf{W}^{(i)}, \mathsf{X}_{\mathsf{R}_k}, \mathbf{V}). \tag{54}$$

And, $g_p(\mathbf{W}, \mathsf{X}_{\mathsf{R}_k}, \mathbf{V})$ in (45a), by following (81) in [32, Eq. (81)] can be upper bounding convex function as

$$g_p(\mathbf{W}, \mathsf{X}_{\mathsf{R}_k}, \mathbf{V}) = j_p^{(i)} - k_p^{(i)}\frac{(\Upsilon_p(\mathbf{W}, \mathsf{X}_{\mathsf{R}_k}, \mathbf{V}))^2}{(|\hat{\mathbf{H}}_{\mathrm{B},p}(\mathsf{X}_{\mathsf{R}_k})\mathbf{W}_p|^2 + \sigma_p^2)^2}, \tag{55}$$

where

$$0 < j_p^{(i)} = \sqrt{1 - 1/(1+\gamma_p^{\varsigma_p}(\mathbf{W}^{(i)}, \mathsf{X}_{\mathsf{R}_k}, \mathbf{V}))^2}/2 + \frac{1}{2\sqrt{1 - 1/(1+\gamma_p^{\varsigma_p}(\mathbf{W}^{(i)}, \mathsf{X}_{\mathsf{R}_k}, \mathbf{V}))^2}}, \tag{56}$$

$$0 < k_p^{(i)} = \big(2\sqrt{1 - 1/(1+\gamma_p^{\varsigma_p,2}(\mathbf{W}^{(i)}, \mathsf{X}_{\mathsf{R}_k}, \mathbf{V})\big)^2}\big)^{-1}. \tag{57}$$

By following Appendix C in [32, Appendix C], we can approximate the lower bound of the RHS term in (55) as

$$\frac{(\Upsilon_p(\mathbf{W}, \mathsf{X}_{\mathsf{R}_k}, \mathbf{V}))^2}{(|\hat{\mathbf{H}}_{\mathrm{B},p}(\mathsf{X}_{\mathsf{R}_k})\mathbf{W}_p|^2 + \sigma_p^2)^2} \geq \frac{4e_p^{(i)}}{(d_p^{(i)})^2}\Omega_p - \frac{2(e_p^{(i)})^2}{(d_p^{(i)})^3} \times \left(|\hat{\mathbf{H}}_{\mathrm{B},p}(\mathsf{X}_{\mathsf{R}_k})\mathbf{W}_p|^2 + \sigma_p^2\right) - \frac{(\Upsilon_p(\mathbf{W}, \mathsf{X}_{\mathsf{R}_k}, \mathbf{V}))^2}{(d_p^2)^2}, \tag{58}$$

where $\Omega_p = \sum_{b\in\mathcal{B}}\big(2\Re\{(\hat{\mathbf{H}}_{\mathrm{B},p}(\mathsf{X}_{\mathsf{R}_k})\mathbf{W}_b^{(i)})^*\hat{\mathbf{H}}_{\mathrm{B},p}(\mathsf{X}_{\mathsf{R}_k})\mathbf{W}_b\} - |\hat{\mathbf{H}}_{\mathrm{B},p}(\mathsf{X}_{\mathsf{R}_k})\mathbf{W}_b^{(i)}|^2\big) + \sum_{p'\in\mathcal{P}\setminus\{p\}}\big(2\Re\{(\hat{\mathbf{H}}_{\mathrm{B},p}(\mathsf{X}_{\mathsf{R}_k})\mathbf{W}_{p'}^{(i)})^* \hat{\mathbf{H}}_{\mathrm{B},p}(\mathsf{X}_{\mathsf{R}_k})\mathbf{W}_{p'}\} - |\hat{\mathbf{H}}_{\mathrm{B},p}(\mathsf{X}_{\mathsf{R}_k})\mathbf{W}_{p'}^{(i)}|^2\big) + \|\hat{\mathbf{H}}_{\mathrm{B},p}(\mathsf{X}_{\mathsf{R}_k})\mathbf{V}\|^2 + \sigma_p^2$, under the trust region constrained by

$$|\hat{\mathbf{H}}_{\mathrm{B},p}(\mathsf{X}_{\mathsf{R}_k})\mathbf{W}_p|^2 + \sigma_p^2 \leq 2d_p^{(i)}, \tag{59a}$$

$$\frac{1}{d_p^{(i)}}\left(|\hat{\mathbf{H}}_{\mathrm{B},p}(\mathsf{X}_{\mathsf{R}_k})\mathbf{W}_p|^2 + \sigma_p^2\right) \leq \frac{2}{e_p^{(i)}}\Omega_p. \tag{59b}$$

By plugging (58) into (55), we have

$$g_p(\mathbf{W}, \mathsf{X}_{\mathsf{R}_k}, \mathbf{V}) \leq j_p^{(i)} - \frac{4e_p^{(i)}k_p^{(i)}}{(d_p^{(i)})^2}\Omega_p + \frac{2(e_p^{(i)})^2k_p^{(i)}}{(d_p^{(i)})^3} \times \left(|\hat{\mathbf{H}}_{\mathrm{B},p}(\mathsf{X}_{\mathsf{R}_k})\mathbf{W}_p|^2 + \sigma_p^2\right) + \frac{\big(\Upsilon_p(\mathbf{W}, \mathsf{X}_{\mathsf{R}_k}, \mathbf{V})\big)^2k_p^{(i)}}{(d_p^{(i)})^2} \triangleq g_p^{(i)}((\mathbf{W}, \mathsf{X}_{\mathsf{R}_k}, \mathbf{V})). \tag{60}$$

From (46) and (60), (45a) can be iteratively re-expressed as

$$r_p(\mathbf{W}, \mathsf{X}_{\mathsf{R}_k}, \mathbf{V}) \geq A\left[\hat{f}_p^{(i)}(\mathbf{W}, \mathsf{X}_{\mathsf{R}_k}, \mathbf{V}) - \xi_p g_p^{(i)}(\mathbf{W}, \mathsf{X}_{\mathsf{R}_k}, \mathbf{V})\right] \triangleq r_p^{(i)}(\mathbf{W}, \mathsf{X}_{\mathsf{R}_k}, \mathbf{V}). \tag{61}$$

And for (45b), the lower bounding concave function for $\hat{f}_{b,p}$ can be approximated as

$$\hat{f}_{b,p}(\mathbf{W}, \mathsf{X}_{\mathsf{R}_k}, \mathbf{V}, \mathbf{P}) \geq \bar{a}_{bp}^{(i)} - |\hat{\mathbf{H}}_{\mathrm{B},b}(\mathsf{X}_{\mathsf{R}_k})\mathbf{W}_p^{(i)}|^2(2\Re\{\Xi_{bp}^{(i)}\})^{-1} - \bar{b}_{bp}^{(i)}|\hat{\mathbf{H}}_{\mathrm{B},b}(\mathsf{X}_{\mathsf{R}_k})\mathbf{W}_p|^2 - \bar{c}_{bp}^{(i)}[\mathbf{P}]_{nf}\Upsilon_{b,p}(\mathbf{W}, \mathsf{X}_{\mathsf{R}_k}, \mathbf{V}, \mathbf{P}) \triangleq \hat{f}_{bp}^{(i)}(\mathbf{W}, \mathsf{X}_{\mathsf{R}_k}, \mathbf{V}, \mathbf{P}). \tag{62}$$

Under the trust region constraint by

$$2\Re\{\Xi_{bp}^{(i)}\} > 0, \tag{63}$$

where

$$\bar{a}_{bp}^{(i)} = \hat{f}_{bp}(\mathbf{W}^{(i)}, \mathsf{X}_{\mathsf{R}_k}, \mathbf{V}, \mathbf{P}) + 2 - \frac{|\hat{\mathbf{H}}_{\mathrm{B},b}(\mathsf{X}_{\mathsf{R}_k})\mathbf{W}_p^{(i)}|^2\sigma_b^2}{d_{bp}^{(i)}e_{bp}^{(i)}}, \tag{64}$$

$$\Xi_{bp}^{(i)} = (\mathbf{W}_p^{(i)})(\mathsf{X}_{\mathsf{R}_k})\hat{\mathbf{H}}_{\mathrm{B},b}\hat{\mathbf{H}}_{\mathrm{B},b}(\mathsf{X}_{\mathsf{R}_k})\mathbf{W}_p - |\hat{\mathbf{H}}_{\mathrm{B},b}(\mathsf{X}_{\mathsf{R}_k})\mathbf{W}_p^{(i)}|^2, \tag{65}$$

$$0 < \bar{b}_{bp}^{(i)} = e_{bp}^{(i)}(d_{bp}^{(i)}|\hat{\mathbf{H}}_{\mathrm{B},b}(\mathsf{X}_{\mathsf{R}_k})\mathbf{W}_p^{(i)}|^2)^{-1}, \tag{66}$$

$$0 < \bar{c}_{bp}^{(i)} = |\hat{\mathbf{H}}_{\mathrm{B},b}(\mathsf{X}_{\mathsf{R}_k})\mathbf{W}_p^{(i)}|^2(d_{bp}^{(i)}e_{bp}^{(i)})^{-1}, \tag{67}$$

$$d_{bp}^{(i)} \triangleq |\hat{\mathbf{H}}_{\mathrm{B},b}(\mathsf{X}_{\mathsf{R}_k})\mathbf{W}_p^{(i)}|^2 + \sigma_b^2, \tag{68}$$

$$e_{bp}^{(i)} \triangleq \big(\sum_{b\in\mathcal{B}} |\hat{\mathbf{H}}_{\mathrm{B},b}(\mathsf{X}_{\mathsf{R}_k})\mathbf{W}_b|^2 + \sum_{p'\in\mathcal{P}\setminus\{p\}} |\hat{\mathbf{H}}_{\mathrm{B},b}(\mathsf{X}_{\mathsf{R}_k})\mathbf{W}_{p'}|^2 + \|\hat{\mathbf{H}}_{\mathrm{B},b}(\mathsf{X}_{\mathsf{R}_k})\mathbf{V}\|^2 + \sigma_b^2\big)[\mathbf{P}]_{nf}. \tag{69}$$

Thus, the function $\hat{f}_p^{(i)}$ in (45b) is concave over the trust region in (47) and it matches with $\hat{f}_p(\mathbf{W}, \mathsf{X}_{\mathsf{R}_k}, \mathbf{V})$ at $\mathbf{W}^{(i)}$:

$$\hat{f}_p^{(i)}(\mathbf{W}^{(i)}, \mathsf{X}_{\mathsf{R}_k}, \mathbf{V}) = \hat{f}_p(\mathbf{W}^{(i)}, \mathsf{X}_{\mathsf{R}_k}, \mathbf{V}). \tag{70}$$

And, $g_{bp}((\mathbf{W}, \mathsf{X}_{\mathsf{R}_k}, \mathbf{V}, \mathbf{P}))$ in (45b) by following (81) in [32, Eq. (81)] can be upper bounded convex function as

$$g_{bp}(\mathbf{W}, \mathsf{X}_{\mathsf{R}_k}, \mathbf{V}, \mathbf{P}) = j_{bp}^{(i)} - k_{bp}^{(i)}\frac{([\mathbf{P}]_{nf}\Upsilon_{bp}(\mathbf{W}, \mathsf{X}_{\mathsf{R}_k}, \mathbf{V}))^2}{(|\hat{\mathbf{H}}_{\mathrm{B},b}(\mathsf{X}_{\mathsf{R}_k})\mathbf{W}_p|^2 + \sigma_b^2)^2}, \tag{71}$$

where

$$0 < j_{bp}^{(i)} = \sqrt{1 - 1/(1+\gamma_b^{\varsigma_p}(\mathbf{W}^{(i)}, \mathsf{X}_{\mathsf{R}_k}, \mathbf{V}, \mathbf{P}))^2}/2 + 1/2\sqrt{1 - 1/(1+\gamma_b^{\varsigma_p}(\mathbf{W}^{(i)}, \mathsf{X}_{\mathsf{R}_k}, \mathbf{V}, \mathbf{P}))^2}, \tag{72}$$

$$0 < k_{bp}^{(i)} = 1/2\sqrt{1 - 1/(1+\gamma_b^{\varsigma_p,2}(\mathbf{W}^{(i)}, \mathsf{X}_{\mathsf{R}_k}, \mathbf{V}, \mathbf{P}))^2}. \tag{73}$$

By following Appendix C in [32, Appendix C], we can approximate the lower bound of the RHS term in (71) as

$$\frac{([\mathbf{P}]_{nf}\Upsilon_{bp}(\mathbf{W}, \mathsf{X}_{\mathsf{R}_k}, \mathbf{V}))^2}{(|\hat{\mathbf{H}}_{\mathrm{B},b}(\mathsf{X}_{\mathsf{R}_k})\mathbf{W}_p|^2 + \sigma_b^2)^2} \geq \frac{4e_{bp}^{(i)}}{(d_{bp}^{(i)})^2}\Omega_{bp} - \frac{2(e_{bp}^{(i)})^2}{(d_{bp}^{(i)})^3} \times \left(|\hat{\mathbf{H}}_{\mathrm{B},b}(\mathsf{X}_{\mathsf{R}_k})\mathbf{W}_p|^2 + \sigma_b^2\right) - \frac{(\Upsilon_{bp}(\mathbf{W}, \mathsf{X}_{\mathsf{R}_k}, \mathbf{V})[\mathbf{P}]_{nf})^2}{(d_{bp}^2)^2}, \tag{74}$$

where $\Omega_{bp} = [\mathbf{P}]_{nf}\big(\sum_{b\in\mathcal{B}}\big(2\Re\{(\hat{\mathbf{H}}_{\mathrm{B},b}(\mathsf{X}_{\mathsf{R}_k})\mathbf{W}_b^{(i)})^*\hat{\mathbf{H}}_{\mathrm{B},b}(\mathsf{X}_{\mathsf{R}_k})\mathbf{W}_b\} - |\hat{\mathbf{H}}_{\mathrm{B},b}(\mathsf{X}_{\mathsf{R}_k})\mathbf{W}_b^{(i)}|^2\big) + \sum_{p'\in\mathcal{P}\setminus\{p\}}(2\Re\{(\hat{\mathbf{H}}_{\mathrm{B},b}(\mathsf{X}_{\mathsf{R}_k})\mathbf{W}_{p'}^{(i)})^*\hat{\mathbf{H}}_{\mathrm{B},p}(\mathsf{X}_{\mathsf{R}_k})\mathbf{W}_{p'}\} - |\hat{\mathbf{H}}_{\mathrm{B},p}(\mathsf{X}_{\mathsf{R}_k})\mathbf{W}_{p'}^{(i)}|^2 + \|\hat{\mathbf{H}}_{\mathrm{B},p}(\mathsf{X}_{\mathsf{R}_k})\mathbf{V}\|^2 + \sigma_b^2\big)$, under the trust region constrained by

$$|\hat{\mathbf{H}}_{\mathrm{B},b}(\mathsf{X}_{\mathsf{R}_k})\mathbf{W}_p|^2 + \sigma_b^2 \leq 2d_{bp}^{(i)}, \tag{75a}$$

$$\frac{1}{d_{bp}^{(i)}}\left(|\hat{\mathbf{H}}_{\mathrm{B},b}(\mathsf{X}_{\mathsf{R}_k})\mathbf{W}_p|^2 + \sigma_b^2\right) \leq \frac{2}{e_{bp}^{(i)}}\Omega_{bp}. \tag{75b}$$

By plugging (74) into (71), we have

$$g_{bp}(\mathbf{W},\mathsf{X}_{\mathsf{R}_k},\mathbf{V},\mathbf{P}) \le j_{bp}^{(i)} - \frac{4e_{bp}^{(i)}k_{bp}^{(i)}}{(d_{bp}^{(i)})^2}\Omega_{bp} + \frac{2(e_{bp}^{(i)})^2k_{bp}^{(i)}}{(d_{bp}^{(i)})^3} \times \left(|\hat{\mathbf{H}}_{\mathrm{B},b}(\mathsf{X}_{\mathsf{R}_k})\mathbf{W}_p|^2+\sigma_b^2\right) + \frac{\left(\Upsilon_{bp}(\mathbf{W},\mathsf{X}_{\mathsf{R}_k},\mathbf{V},\mathbf{P})\right)^2k_{bp}^{(i)}}{(d_{bp}^{(i)})^2} \triangleq g_{bp}^{(i)}((\mathbf{W},\mathsf{X}_{\mathsf{R}_k},\mathbf{V},\mathbf{P})). \tag{76}$$

From (62) and (76), (45b) can be iteratively re-expressed as

$$r_p(\mathbf{W},\mathsf{X}_{\mathsf{R}_k},\mathbf{V},\mathbf{P}) \ge A\Big[\hat{f}_{bp}^{(i)}(\mathbf{W},\mathsf{X}_{\mathsf{R}_k},\mathbf{V},\mathbf{P}) - \xi_p g_{bp}^{(i)}(\mathbf{W},\mathsf{X}_{\mathsf{R}_k},\mathbf{V},\mathbf{P})\Big] \triangleq r_{bp}^{(i)}(\mathbf{W},\mathsf{X}_{\mathsf{R}_k},\mathbf{V},\mathbf{P}). \tag{77}$$

We move to the approximation of constraint (19d) which can be re-expressed from (12) as

$$|\hat{\mathbf{H}}_{\mathrm{B},b}(\mathsf{X}_{\mathsf{R}_k})\mathbf{W}_b|^2 \ge \zeta_b^{-1}\Upsilon_b(\mathbf{W},\mathsf{X}_{\mathsf{R}_k},\mathbf{V},\mathbf{P}). \tag{78}$$

To get a tractable form, we introduce new variables $\mathbf{\Lambda} \triangleq \{\Lambda_{b,p} \ge 0\}$ which satisfy the convex constraint $\Lambda_{b,p'} \ge |\hat{\mathbf{H}}_{\mathrm{B},b}(\mathsf{X}_{\mathsf{R}_k})\mathbf{W}_b|^2$. Then, the (78) can be re-expressed as

$$|\hat{\mathbf{H}}_{\mathrm{B},b}(\mathsf{X}_{\mathsf{R}_k})\mathbf{W}_b|^2 \ge \zeta_b^{-1}\Big(\sum_{b'\in\mathcal{B}\setminus\{b\}}|\hat{\mathbf{H}}_{\mathrm{B},b}(\mathsf{X}_{\mathsf{R}_k})\mathbf{W}_{b'}|^2 + \|\hat{\mathbf{H}}_{\mathrm{B},b}(\mathsf{X}_{\mathsf{R}_k})\mathbf{V}\|^2+\sigma_b^2+\sum_{p'\in\mathcal{P}}\big(1-[\mathbf{P}]_{bp'}\big)\Lambda_{b,p'}\Big) \triangleq \zeta_b^{-1}\hat{\Upsilon}_b(\mathbf{W},\mathsf{X}_{\mathsf{R}_k},\mathbf{V},\mathbf{P},\mathbf{\Lambda}). \tag{79}$$

By following Lemma 1, the LHS of (79) can be approximated as

$$|\hat{\mathbf{H}}_{\mathrm{B},b}(\mathsf{X}_{\mathsf{R}_k})\mathbf{W}_b|^2 \ge 2\Re\left\{(\hat{\mathbf{H}}_{\mathrm{B},b}(\mathsf{X})\mathbf{W}_b^{(i)})^*(\hat{\mathbf{H}}_{\mathrm{B},b}(\mathsf{X})\mathbf{W}_b)\right\} - |\hat{\mathbf{H}}_{\mathrm{B},b}(\mathsf{X})\mathbf{W}_b|^2 \triangleq f_b^{(i)}(\mathsf{X},\mathbf{W}_b), \tag{80}$$

And, the $\Upsilon_b(\mathbf{W},\mathsf{X},\mathbf{V},\mathbf{P},\mathbf{\Lambda})$ by following Lemma 2 can iteratively determine the upper bound as

$$\hat{\Upsilon}_b(\mathbf{W},\mathsf{X},\mathbf{V},\mathbf{P},\mathbf{\Lambda}) \le \sum_{p'\in\mathcal{P}}\frac{1}{2}\left(\frac{(1-[\mathbf{P}]^{(i)})\Lambda_{b,p'}^2}{\Lambda_{b,p'}^{(i)}}+\frac{\Lambda_{b,p'}^{(i)}(1-[\mathbf{P}]_{bp'})}{1-[\mathbf{P}]_{b,p'}^{(i)}}\right) + \sum_{b'\in\mathcal{B}\setminus\{b\}}|\hat{\mathbf{H}}_{\mathrm{B},b}(\mathsf{X})\mathbf{W}_{b'}|^2+\|\hat{\mathbf{H}}_{\mathrm{B},b}(\mathsf{X})\mathbf{V}\|^2+\sigma_b^2 \triangleq \hat{\Upsilon}_b^{(i)}(\mathbf{W},\mathsf{X},\mathbf{V},\mathbf{P},\mathbf{\Lambda}). \tag{81}$$

Noteworthy that $\Upsilon_b(\mathbf{W},\mathsf{X},\mathbf{V},\mathbf{P},\mathbf{\Lambda})$ is global upper bound and $\Upsilon_b^{(i)}(\mathbf{W},\mathsf{X},\mathbf{V},\mathbf{P},\mathbf{\Lambda})$ is quadratic convex function, which is satisfying $\Upsilon_b^{(i)}(\mathbf{W},\mathsf{X},\mathbf{V},\mathbf{P},\mathbf{\Lambda}) = \Upsilon_b^{(i)}(\mathbf{W}^{(i)},\mathsf{X}^{(i)},\mathbf{V}^{(i)},\mathbf{P}^{(i)},\mathbf{\Lambda}^{(i)})$. Accordingly, by following convex constraint, (79) iteratively can be re-expressed as

$$\zeta_b^{-1}\hat{\Upsilon}_b(\mathbf{W},\mathsf{X},\mathbf{V},\mathbf{P},\mathbf{\Lambda}) \le f_b^{(i)}(\mathsf{X},\mathbf{W}_b). \tag{82}$$

Currently, we tackle constraint (19e). Without loss generality, from (14), we can rewrite constraint (19e) as

$$\zeta_p^{-1} \le \frac{|\hat{\mathbf{H}}_{\mathrm{B},p}(\mathsf{X})\mathbf{W}_p|^2}{\Upsilon_p(\mathbf{W},\mathsf{X},\mathbf{V})}, \tag{83a}$$

$$\zeta_p^{-1} \le \frac{|\hat{\mathbf{H}}_{\mathrm{B},b}(\mathsf{X})\mathbf{W}_p|^2}{[\mathbf{P}]_{nf}\Upsilon_{b,p}(\mathbf{W},\mathsf{X},\mathbf{V})}. \tag{83b}$$

Inequality (83a) can be re-written as

$$\zeta_p^{-1}\Upsilon_p(\mathbf{W},\mathsf{X},\mathbf{V}) \le |\hat{\mathbf{H}}_{\mathrm{B},p}(\mathsf{X})\mathbf{W}_p|^2, \tag{84}$$

by following Lemma 1, the RHS term of inequality (84) can be lower bounded as

$$|\hat{\mathbf{H}}_{\mathrm{B},p}(\mathsf{X})\mathbf{W}_p|^2 \ge 2\Re\left\{(\hat{\mathbf{H}}_{\mathrm{B},p}(\mathsf{X})\mathbf{W}_p^{(i)})^*(\hat{\mathbf{H}}_{\mathrm{B},p}(\mathsf{X})\mathbf{W}_p)\right\} - |\hat{\mathbf{H}}_{\mathrm{B},p}(\mathsf{X})\mathbf{W}_p|^2 \triangleq f_p^{(i)}(\mathsf{X},\mathbf{W}_p), \tag{85}$$

also, noteworthy that the LHS of (84) is a function of quadratic-over-linear, and it is convex. Thus, we can approximate (83a) at iteration $i+1$ as

$$\zeta_p^{-1}\Upsilon_p(\mathbf{W},\mathsf{X},\mathbf{V}) \le f_p^{(i)}(\mathsf{X},\mathbf{W}_p). \tag{86}$$

Similar to (83a), (83b) can be approximated as

$$\zeta_p^{-1}\Upsilon_{b,p}(\mathbf{W},\mathsf{X},\mathbf{V}) \le |\hat{\mathbf{H}}_{\mathrm{B},b}(\mathsf{X})\mathbf{W}_p|^2[\mathbf{P}]_{nf}^{-1}, \tag{87}$$

where the RHS and LHS terms are a quadratic-over-linear function. So, by following Lemma 1 again, we tackle the RHS term of (87) can be lower bound as

$$|\hat{\mathbf{H}}_{\mathrm{B},b}(\mathsf{X})\mathbf{W}_p|^2[\mathbf{P}]_{nf}^{-1} \ge \frac{2\Re\left\{(\hat{\mathbf{H}}_{\mathrm{B},b}(\mathsf{X})\mathbf{W}_p^{(i)})^*(\hat{\mathbf{H}}_{\mathrm{B},b}(\mathsf{X})\mathbf{W}_p)\right\}}{[\mathbf{P}]_{nf}^{(i)}} - |\hat{\mathbf{H}}_{\mathrm{B},b}(\mathsf{X})\mathbf{W}_p^{(i)}|^2[\mathbf{P}]_{nf}(|[\mathbf{P}]_{nf}|)^{-2} \triangleq f_{b,p}^{(i)}(\mathsf{X},\mathbf{W}_p,[\mathbf{P}]_{nf}). \tag{88}$$

Thus, by following convex constraint, (83b) iteratively can be re-expressed as

$$\zeta_p^{-1}\Upsilon_{b,p}(\mathbf{W},\mathsf{X},\mathbf{V}) \le f_{b,p}^{(i)}(\mathsf{X},\mathbf{W}_p,[\mathbf{P}]_{nf}). \tag{89}$$

From (19f) and (19g), the LHS terms are logarithmic function and convex while the RHSs are linear. To address these inequalities, we convert and approximate them into SOC constraints. The LHS term $\ln(1+\zeta_u^{-1})$, where $\zeta_u \in \{\zeta_b,\zeta_p\}$, with $\zeta_u > 0$ can be approximate at iteration $i+1$ by implementing equation (66) which is the concave lower bound of the logarithmic function in [40, (66)] as

$$\ln(1+\zeta_u^{-1}) \ge \ln(1+(\zeta_u^{(i)})^{-1}) + (\zeta_u^{(i)}+1)^{-1} - \zeta_u[\zeta_u^{(i)}(\zeta_u^{(i)}+1)]^{-1} \triangleq \mathcal{D}^{(i)}(\zeta_u). \tag{90}$$

Thus, the problem (22) can be approximate at $i+1$ iteration by following convex problem:

$$\max_{\substack{\mathbf{W},\mathbf{V},\mathbf{P},\\ \mathbf{r},\boldsymbol{\zeta},\mathbf{\Lambda}}} \ \bar{\mathcal{R}}_{\Sigma}^{(i)} \triangleq \sum_{b\in\mathcal{B}}r_b+\sum_{p\in\mathcal{P}}r_p \tag{91a}$$

$$\text{s.t. } \mathcal{D}^{(i)}(\zeta_b)\ge r_b,\ \mathcal{D}^{(i)}(\zeta_p)\ge r_p, \tag{91b}$$

$$|\hat{\mathbf{H}}_{\mathrm{B},b}(\mathsf{X}_{\mathsf{R}_k})\mathbf{W}_b|^2 \le \Lambda_{b,p'}, \tag{91c}$$

$$(17c),(17f),(30),(42a),(42b),(47),(59a),(59b),(27),(82),(86),(89),(90),(63),(75a),(75b). \tag{91d}$$

After addressing problem (91), we obtain an optimal solution for $[\mathbf{P}]$ that consists of non-integer values. This means that the optimal solution obtained from problem (91) is not feasible for the original problem (17). Similar to phase shift issue, we apply a rounding function (21) after obtaining the optimal solution to the problem (91) to address this issue with $\mathsf{Y} \triangleq [\mathbf{P}]_{bp}^{\star}$ and $\alpha = 0.5$.

In the end, we summarize the proposed low-complexity iterative algorithm to solve the beamforming problem (91) in Algorithm 2. The initial point is generated randomly with $A > 100$ [36], so that the Algorithm 2 always initializes with a feasible solution of (91). Our transformations from the original problem (17) to problem (91) are illustrated in Fig. 2.

IV. Deep Learning Framework for SEM Problem

In STAR-RIS-assisted MIMO-NOMA systems, the complexity of determining the resource allocation constantly in-

Algorithm 2 Proposed IA-based for solving problem (17)

Output: $\mathbf{W}^\star$, $\mathbf{V}^\star$, $\mathbf{P}^\star$, $\mathbf{\Psi}^\star_{\mathrm{R}_k}$, $\mathbf{\Theta}^\star_{\mathrm{R}_k}$, $\mathcal{R}_{\sum}$.

1: **Initialization:**
Set $(\mathbf{W}^\star, \mathbf{V}^\star, \mathbf{P}^\star) \leftarrow 0$, and generate random initial feasible point $(\mathbf{W}^{(0)}, \mathbf{V}^{(0)}, \mathbf{P}^{(0)} \boldsymbol{\zeta}^{(0)}, \Lambda^{(0)})$ for (22), $\alpha = 0.5$.
2: **repeat**
3: Solve the convex problem (20), to find $(\mathbf{\Psi}^\star_{\mathrm{R}_k}, \mathbf{\Theta}^\star_{\mathrm{R}_k})$ based on Algorithm 1.
4: Solve the convex problem (91), to find $(\mathbf{W}^\star, \mathbf{V}^\star, \mathbf{P}^\star\ \boldsymbol{\zeta}^\star, \mathbf{\Lambda}^\star)$;
5: Update variable based on $(\mathbf{W}^\star, \mathbf{V}^\star, \mathbf{P}^\star, \boldsymbol{\zeta}^\star, \mathbf{\Lambda}^\star)$;
6: **until** Convergence
7: Round up $(\mathbf{P}^\star)$ based on (21);
8: Update $(\mathbf{W}^\star, \mathbf{V}^\star, \mathbf{P}^\star, \mathbf{\Psi}^\star_{\mathrm{R}_k}, \mathbf{\Theta}^\star_{\mathrm{R}_k}) \leftarrow (\mathbf{W}^{(i)}, \mathbf{V}^{(i)}, \mathbf{P}^{(i)}, \mathbf{\Psi}^{(i)}_{\mathrm{R}_k}, \mathbf{\Theta}^{(i)}_{\mathrm{R}_k})$;
9: Calculate $\mathcal{R}_{\sum}$ in (19) based on $(\mathbf{W}^\star, \mathbf{V}^\star, \mathbf{P}^\star, \mathbf{\Psi}^\star_{\mathrm{R}_k}, \mathbf{\Theta}^\star_{\mathrm{R}_k})$.

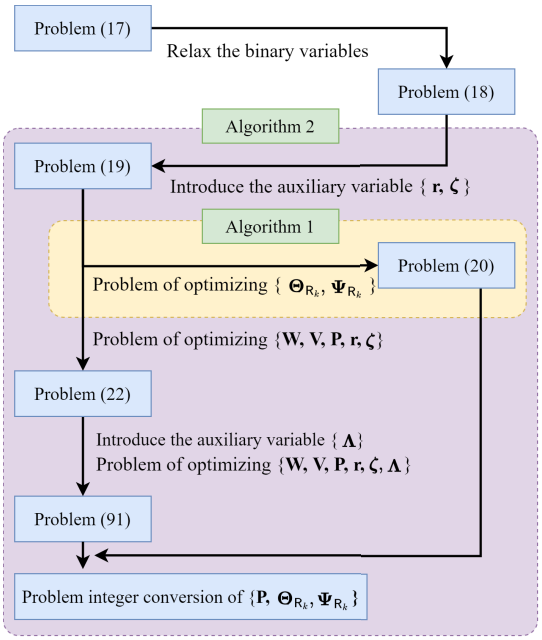

Fig. 2. Illustration of the transformation flow for the formulated optimization problem.

creases when the number of users increases. Moreover, the conventional approach faces resource optimization challenges in determining optimal solutions efficiently. To address this problem, we propose the DL framework based on the CNN model to predict the optimal solution from unknown data sets.

We design the proposed DL framework to predict the optimal solution including offline learning and online predicting, as shown in Fig. 3. Compared to the fully connected deep neural network (DNN), the CNN can reduce the number of learning parameters due to the CNN adopting the sharing parameters so that it can extract features effectively [10]. Different from the conventional approach to solving the problem (20) and (91), which requires some iteration, we consider the input variables of the CNN model including the positional information for energy users ($\mathrm{E}_q^{\mathrm{Pos}}$), near information users ($\mathrm{ID}_n^{\mathrm{Pos}}$), and far information users ($\mathrm{ID}_f^{\mathrm{Pos}}$) - and for STAR-RISs ($\mathrm{R}_k^{\mathrm{Pos}}$), the number of energy users (Q), the number of near and far information users (N, F), the number of STAR-RISs (K), the number of BS's antennas (M_{BS}), the number of STAR-RISs elements (L), blocklength (A), transmit power at the BS ($\bar{P}_{\mathrm{BS}}$), the channel coefficient matrix from BS to STAR-RIS ($\mathbf{H}_{\mathrm{BS},\mathrm{R}_{k,r}}$, $\mathbf{H}_{\mathrm{BS},\mathrm{R}_{k,t}}$), channel coefficient matrix from STAR-RIS to information users, ($\mathbf{H}_{\mathrm{R}_{k,r},\mathrm{ID}_n}$, $\mathbf{H}_{\mathrm{R}_{k,t},\mathrm{ID}_f}$), and channel coefficient vector from BS to energy users, ($\mathbf{h}_{\mathrm{BS},\mathrm{E}_q}$). Based on these settings, the linear precoding matrix $\mathbf{W}$, the phase shift of reflection $\mathbf{\Theta}_{\mathrm{R}_k}$ and transmission $\mathbf{\Psi}_{\mathrm{R}_k}$ at STAR-RIS, energy beamforming matrix $\mathbf{V}$, and user grouping $\mathbf{P}$, which are achieved by solving the problem (86) via Algorithm 2 and then arranged into a matrix $\mathbf{Y} \triangleq [\mathbf{W}, \mathbf{\Theta}_{\mathrm{R}_k}, \mathbf{\Psi}_{\mathrm{R}_k}, \mathbf{V}, \mathbf{P}]$, serve as output variables of CNN. The whole dataset having 10K samples is divided randomly into the training, validations, and test sets with a ratio of 80-10-10.

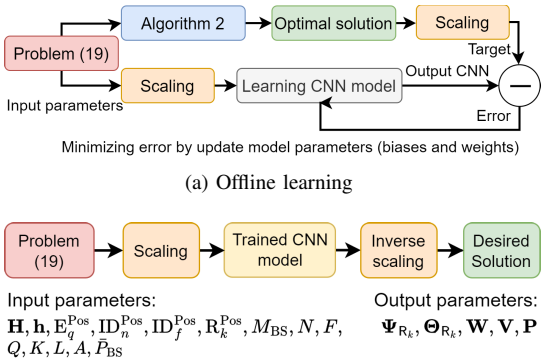

(a) Offline learning

(b) Online predicting

Fig. 3. The proposed DL framework to predict the optimal value.

Fig. 3(a) shows the CNN model that learns by offline the relationship between input parameters from the problem (19) and the optimal solution as a target obtained by solving the problem (19) with Algorithm 2. The training dataset is normalized as $\mathbf{y} = (\mathbf{y} - \min(\mathbf{y}))/(\max(\mathbf{y}) - \min(\mathbf{y}))$ with dimension $(L_r \times M_{\mathrm{BS}}) + (L_t \times M_{\mathrm{BS}}) + (M_n \times L_r) + (M_f \times L_t) + (1 \times M_{\mathrm{BS}}) + Q(2\times 1) + N(2\times 1) + F(2\times 1) + K(2\times 1) + M_{\mathrm{BS}} + 8$ before the learning process to improve the convergence speed and avoid numerical instabilities. During offline learning, the DL framework continually improves the CNN model by updating model parameters (biases and weights) to minimize errors between the output CNN model and the target. The resulting CNN is employed as a mapping function to predict online the optimal solution whenever the new input parameters are available as shown in Fig. 3(b). In the prediction step, we also implement scaling to maintain consistent feature representation. Following the prediction process, the inverse scaling is performed to obtain the real value of output parameters. This process significantly reduces the computational complexity due to the complexity being transferred to offline learning.

The designed CNN architecture shown in Fig. 4 includes an input layer, the convolution layer (CL), batch normalization (BN) layers, an activation (AC) layer, a flatten layer, a fully connected (FC) layer, and an output layer. The CL, BN, and AC layers can be grouped into convolution blocks (CB). Thus, stacking multiple convolution blocks allows the model

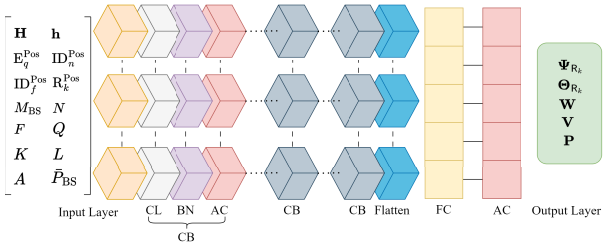

Fig. 4. The proposed architecture of the CNN model.

to learn more complex features from the input parameters. Additionally, due to the balance between model complexity and efficiency, we consider 3 CB layers in the proposed architecture of the CNN model. In the dimensional layer size of the layer structure, we consider 1 input layer is 1×56, CL is 1×16 with 256 neurons while the output layer is 1×70. In this model, we consider rectified linear unit (ReLU) for the AC layers. Before passing the feature to the FC layer, the features are flattened into a vector. The FC layer combines all features to make the final prediction decision.

V. The Proposed SEM Algorithm Complexity Analysis

We are now in the process of outlining the worst-case per-iteration complexity analysis of the proposed Algorithms 1 and 2. As explained above, an advantage of the proposed algorithms is the complexity of solving the convex problem. Algorithms 1 and 2 for the convex phase shift and beamforming optimization problems have a low computational complexity, which only involves SOC and linear constraints. Moreover, the brute-force search (BFS) algorithm is also provided as the optimal scheme for benchmark purposes. We denote λ_c, τ_c and $\mathcal{O}_c$ as the numbers of linear/SOC constraints, scalar optimization, and worst-case per-iteration where $c \in \{1, 2\}$ with c = 1 being Algorithm 2 and c = 2 being BFS algorithm, respectively. We summarize the worst-case complexity of the proposed algorithm in Table II. As can be observed, the BFS algorithm finds the best user-grouping within $\max(N, F)!/(|N - F|)!$ possibilities. The complexity of each subproblem in the BFS algorithm can be calculated in the same way as Algorithm 2 but without the user binary variable. The numbers of scalar optimization variables and linear/SOC constraints in the BFS algorithm are $\tau_2 = (M_{\text{BS}} + 3)(NM_n + FM_f) + (M_{\text{BS}}\bar{Q})$ and $\lambda_2 = 2K^L + 2NF + 3(NM_n + FM_f) + Q + 1$, respectively. Therefore, the total complexity of the BSF algorithm is $\max(N, F)!/(|N-F|)! \times \mathcal{O}(\tau_2^2\lambda_2^{2.5} + \lambda_2^{3.5})$, which indicates that the complexity of the BFS scheme has very high complexity even for medium-sized networks. Thus, the BFS algorithm is only served as a benchmark scheme.

VI. Numerical Results

In this section, we provide illustrative numerical results to evaluate the proposed algorithm and the DL approach in improving the SE performance in the networks. We consider the downlink network topology with the cell radius d_1, d_2, and d_3 as 100, 200, and 300 m, respectively. Unless otherwise stated, we set in simulations the number of energy users

TABLE II
The Complexity Analysis of The Proposed Algorithm 2 and BFS Algorithm.

τ_1	$(M_{\text{BS}} + 3)(NM_n + FM_f) + NF + M_{\text{BS}}Q + KL$
λ_1	$(NM_n + FM_f)(2NF + 1) + 3NF + 4(N + F) + Q + 1$
$\mathcal{O}_1$	$\tau_1^2\lambda_1^{2.5} + \lambda_1^{3.5}$
τ_2	$(M_{\text{BS}} + 3)(NM_n + FM_f) + (M_{\text{BS}}Q)$
λ_2	$2K^L + 2NF + 3(NM_n + FM_f) + Q + 1$
$\mathcal{O}_2$	$\max(N, F)!/(\lvert N - F\rvert)! \times (\tau_2^2\lambda_2^{2.5} + \lambda_2^{3.5})$

$Q = 4$, the number of near information users is set to $N = 3$, and the number of far information users is set to $F = 5$. The energy users, near information users, and far information users are uniformly deployed in zones 1, 2, and 3, respectively. The number of STAR-RISs is set to $K = 4$, with each STAR-RIS having 20 transmission elements ($L_t = 20$) and 20 reflection elements ($L_r = 20$), and they are deployed between zones 2 and 3. The number of antennas at BS, near and far information users $M_{\text{BS}} = 10$, $M_n = 2$, $M_f = 2$, respectively. The blocklength (number of channel uses) $A = 1000$, the instantaneous BLER at ID_n and ID_f $\varpi_b = \varpi_p = 10^{-5}$ [41], the target energy harvesting threshold at E_q $\bar{\text{E}}_q = -55$ dBm, target SE threshold at ID_b and ID_p $\bar{\text{R}}_b = \bar{\text{R}}_p = 1$bps/Hz and the threshold BLER at ID_b and ID_p $\bar{\varpi}_b = \bar{\varpi}_p = 10^{-4}$ [1], [2]. We set the pathloss exponent $\sigma_{\text{PL}} = 2.7$ [11] and Rician factor $\mathsf{k} = 3$ dB [27]. We use SDPT3 as a convex solver and YALMIP toolbox in the MATLAB software to solve the convex problem. Additionally, MATLAB software is used to implement the designed CNN model for fairness comparison. The SE result is obtained in nats/sec/Hz, which can be divided by $\ln(2)$ to get the result in bits/sec/Hz.

We investigate the performance of the proposed AUG scheme by comparing it with the RUG (two information users will be grouped randomly) and NUG (no information users will be grouped) which serve as benchmark schemes. By setting the matrix $\mathbf{P}$ in (91) to one or zero, the proposed algorithm can be switched into the RUG or NUG schemes, respectively. The benchmark schemes can be simulated using the same algorithms in this setting. We illustrate in Fig. 5(a) the convergence of the proposed Alg. 1. As can be observed in Fig. 5(a), the convergence behavior of Alg. 1 is obtained within 8 iterations because every iteration of the proposed algorithm can search for a better solution of SE from the whole feasible set, which shows the effectiveness of Alg. 1 in solving a problem (17).

Fig. 5(b) shows the convergence behavior of Algorithm 2 with different schemes, where the results are obtained by averaging 1000 random channel realization with $\bar{P}_{\text{BS}} = 30$ dBm. Alg. 2 converges within 8 iterations because it can find an improved solution in each iteration, indicating its effectiveness. The AUG scheme outperforms the RUG and NUG ones because it can find the most potential information users in zones 2 and 3, under the same STAR-RIS and beamforming. The AUG groups users only if their SINR improves, while the RUG randomly groups users without considering their location, and NUG scheme serves all users individually. In the NUG, the lack of grouping leads to higher SINR interference, reducing performance. RUG suffers from a similar issue since

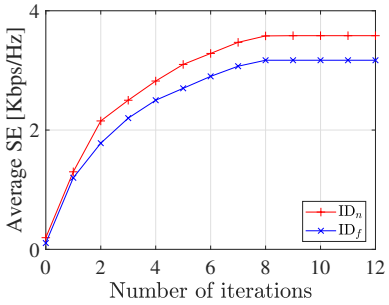

(a) Convergence of Alg. 1 for ID_n and ID_f.

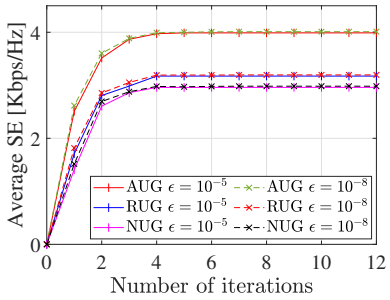

(b) Convergence of Alg. 2 for all schemes.

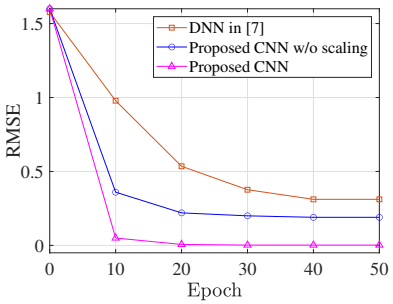

(c) Impact of the epoch on the RMSE.

Fig. 5. Convergence of Alg. 1, Alg. 2 and RMSE versus epoch.

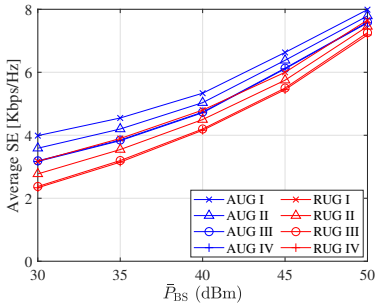

(a) Average SE vs. $\bar{P}_{\mathrm{BS}}$ with various scenarios.

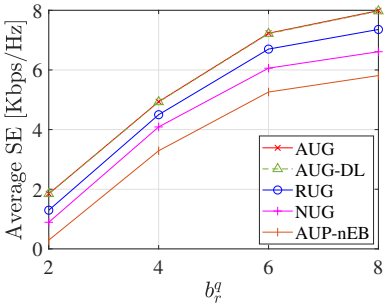

(b) Average SE versus b_r^q.

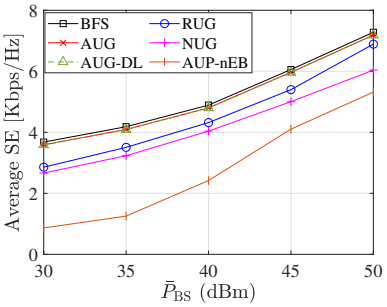

(c) Average SE versus $\bar{P}_{\mathrm{BS}}$

Fig. 6. Impact of the $\bar{P}_{\mathrm{BS}}$ with various scenarios, b_r^q, and $\bar{P}_{\mathrm{BS}}$ on the average SE.

it randomly selects users for pairing. This corresponds to (12) and (14), wherein the $[\mathbf{P}]_{nf} = 0$, consequently, the interference of SINR is high. Additionally, when the convergence rate decreases, the iteration of Alg. 2 to achieve the optimal values increases from 8 to 10 iterations, and the SE performance increases slightly. The reason is that when Alg. 2 is closer to the optimal value, the improvements become smaller. Thus, it needs more iteration to achieve the optimal values precisely; however, there is a slight improvement in the SE performance of the system.

Fig. 5(c) reveals the root mean square error (RMSE) as a function of epoch. This metric shows the accuracy between the optimal value predictions and the actual data in the test set [42], which can be expressed as

$$\mathrm{RMSE}(\tau^{(n)}, \widetilde{\tau}^{(n)}) = \sqrt{\frac{1}{\widetilde{N}} \sum_{n=1}^{\widetilde{N}} (\tau^{(n)} - \widetilde{\tau}^{(n)})^2}, \tag{92}$$

where $\widetilde{N}$ denotes the number of samples in the test set, $\tau^{(n)}$ is predicted optimal value while $\widetilde{\tau}^{(n)}$ is an output of the test set. A smaller RMSE indicates that the predicted and observed optimal values more closely match, implying high accuracy. As can be observed in Fig. 5(c), RMSE decreases as the number of epochs increases due to the CNN model updating its biases and weights. The conventional DNN has the highest RMSE, while the proposed CNN achieves the lowest RMSE. The reason is that the CNN reduces shared parameters compared to a fully connected DNN. Additionally, the CNN with scaling performs better than the one without scaling. The scaling block normalizes input and output parameters, stabilizing the learning process and preventing the gradient from vanishing or exploding.

TABLE III
THE CELL RADIUS IN VARIOUS SCENARIOS

Scenario	d_1 (m)	d_2 (m)	d_3 (m)
I	100	100	100
II	150	50	100
III	50	100	150
IV	50	150	100

We now analyze the impact of the dimension size on each zone with the variation of $\bar{P}_{\mathrm{BS}}$ of the proposed AUG scheme. We consider the cell radius with different scenarios as shown in the Table. III. Fig. 6(a) reveals the impact of $\bar{P}_{\mathrm{BS}}$ on the average SE in various scenarios. As can be observed in Fig. 6(a), the AUG scheme outperforms the RUG schemes. It is not surprising because the AUG scheme finds the optimal information users in different zones to be grouped to achieve the maximum SE, while the RUG randomly groups the information users, and it achieves the lower SE performance. Furthermore, the AUG and RUG schemes with scenario I outperform their counterparts with the remaining scenarios. In scenario I, a balanced configuration would potentially offer a uniform distribution of signal quality across the cell. Each zone, including energy users and information users, has almost the same distance range, leading to a possibly more consistent SE performance across the entire cell. Scenario II obtains the

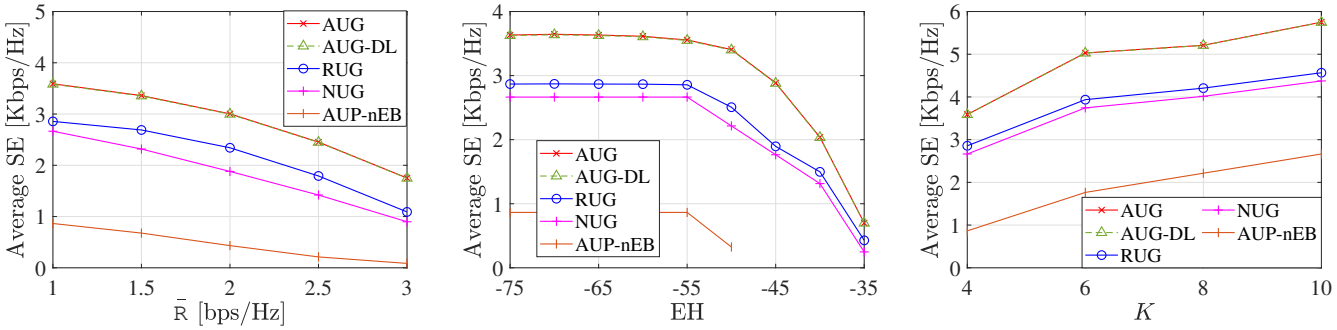

(a) Average SE versus minimum data rates $\bar{\mathrm{R}}$ (b) Average SE versus $\bar{\mathrm{E}}$ (c) Average SE versus K

Fig. 7. Impact of $\bar{\mathrm{R}}$, $\bar{\mathrm{E}}$, and K on average SE.

second SE performer due to the BS needing more energy to serve the energy users but still within a reasonable range from STAR-RIS to serve information users. The scenarios III and IV make the schemes under consideration to have the worst performance since the ID_f of scenario III and ID_n of scenario IV would experience more path loss. Moreover, due to the potential benefit of STAR-RIS, ID_n becomes a far information user, and ID_f becomes a near information user. Besides that, the energy users are close to the BS, ensuring efficient energy transfer, which improves the SE performance.

Fig. 6(b) analyzes the effect of the number of STAR-RIS quantization levels on the average SE performance. When the number of quantization levels at the STAR-RIS increases, the average SE improves. The reason is that higher quantization levels allow more precise phase adjustments, which can lead to better signal alignment and reduced interference. Again, the AUG scheme is the best performer, and the AUG-DL scheme shows an excellent ability to predict optimal solutions.

Fig. 6(c) shows the impact of $\bar{P}_{\mathrm{BS}}$ on the average SE. When the $\bar{P}_{\mathrm{BS}}$ increases, the average SE increases since the higher power at the BS supports more information users. The BFS scheme performs best by finding the best information user to be grouped among all possibilities, but its high complexity increases exponentially with more users. In contrast, the AUG scheme, with low complexity, performs similarly, with only a 2.6% deviation, as illustrated in Table IV. This deviation is due to applying the rounding function (21) after obtaining the optimal solution. AUG outperforms RUG and NUG, as it optimally groups users in different zones, while the RUG randomly groups users and no user grouping is in NUG, resulting in poorer performance. We also demonstrate the system without energy beamforming, labeled as "AUG-nEB", by setting the matrix $\mathbf{V}$ to zeros. In AUG-nEB, the BS must share a portion of its energy to power the energy users to satisfy the constraint (17b), decreasing the SE. This highlights the importance of energy beamforming design. In addition, the AUG-DL scheme provides a curve that fits the average SE to the AUG scheme; thus, the DL has a good ability to predict the output parameters with good accuracy.

Figs. 7(a) and 7(b) show effects of the minimum data rate $\bar{\mathrm{R}}$ and threshold $\bar{\mathrm{E}}$ on the average SE performance of all schemes with $\bar{P}_{\mathrm{BS}} = 30$ dBm and $\bar{\mathrm{R}} = 1$ bps/Hz. As can be observed

TABLE IV
THE AVERAGE SE OF THE AUG AND BFS SCHEMES ON $\bar{P}_{\mathrm{BS}}$

P_{BS} [dBm]	30	35	40	45	50
AUG [Kbps/Hz]	3.5897	4.0937	4.7869	5.9669	7.1894
BFS [Kbps/Hz]	3.6795	4.1835	4.8914	6.0567	7.2792

in Figs. 7(a) and 7(b), the AUG provides the best average SE performance while the AUG-nEB is the worst performer. In the AUG-nEB, the BS has to share its energy to power the energy users while still guaranteeing QoS constraints of information users. Therefore, the portion of energy for data transmission is reduced, which results in low SE performance. In the NUG scheme, the BS allocates a significant portion of its power budget to serve near and far information users independently. Consequently, the SE decreases when the data rate requirements for information users are increased. In contrast, the RUG scheme provides a higher SE performance since the information users in the group can mitigate interference from the other one in the group. Nevertheless, selecting two users randomly to a group is not a favorable method when they are in the same zone. As described in Remark 1, the AUG scheme addresses this problem by optimally selecting two information users with differing channel conditions for grouping, thereby quickly achieving a satisfactory solution for information user grouping and energy user constraints. This enables the system to maintain its QoS requirements even in high data rate regime scenarios. Furthermore, Fig. 7(b) shows that the gap of average SE of all schemes is narrow in high $\bar{\mathrm{E}}$. In the AUG scheme, it significantly decreases starting from -50 dBm while other schemes start from -55 dBm. Particularly, the average SE of all schemes is infeasible with the high impact of $\bar{\mathrm{E}}$ on the system when $\bar{\mathrm{E}}$ is larger than -35 dBm. For $\bar{\mathrm{E}}$ less than -35 dBm, which indicates small $\bar{\mathrm{E}}$, the received signal still can fulfill the harvested power requirement. In this case, the BS primarily allocates its power to information users. Nevertheless, for the large $\bar{\mathrm{E}}$, BS needs to allocate more power to energy users due to (17b) being feasible, which results in the decrease of the received power of information users and the average SE in the system. Furthermore, the performance of the AUG scheme outperforms the RUG and NUG schemes, which shows the effectiveness of the proposed scheme applying to the MIMO-

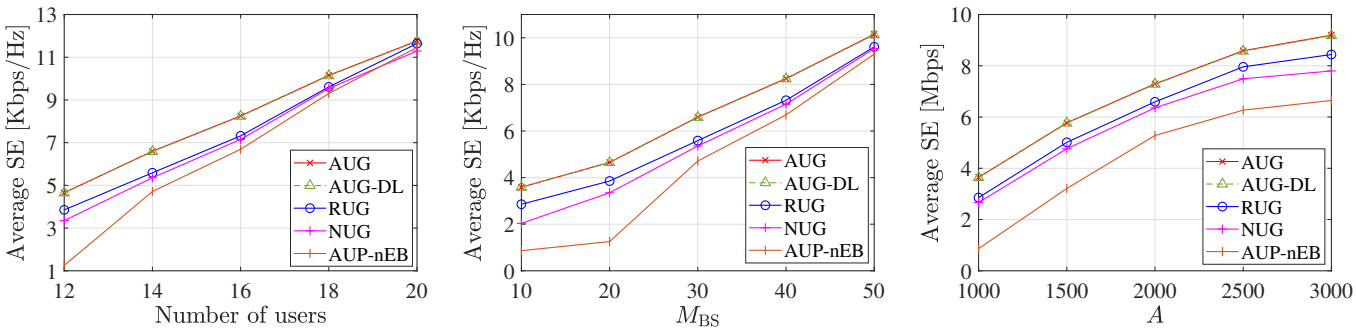

(a) Average SE versus the total number of users (b) Average SE versus M_{BS} (c) Average SE versus A

Fig. 8. Impact of the number of users, M_{BS} and A on average SE.

NOMA network under NL-EH circuit conditions.

Fig. 7(c) plots the average SE versus the number of STAR-RIS, K, with various schemes. As expected, the average SE of all schemes increases when K increases because the use of using STAR-RIS can increase the system's degree of freedom (DoF). By doing so, the STAR-RIS can significantly improve the signal quality of the users. Again, the AUG scheme has the highest SE performance among the considered schemes, and the AUG-DL can present good predictive ability.

Fig. 8 plots the average SE versus the number of users, the number of BS's antenna (M_{BS}), and blocklength (A). As can be observed in Fig. 8, when the number of users, M_{BS}, and A increases, the average SE increases. As expected, the average SE improves when the number of users and M_{BS} increases because DoF from M_{BS} still contributes to the system. In low M_{BS}, the gap between AUG and NUG is high compared to the high M_{BS} due to low DoF in low M_{BS} the NOMA system becomes important. In contrast, when M_{BS} increases, the gap between AUG and NUG decreases due to the contribution of DoF, and the effect of interference-free becomes less significant in the NUG scheme. Consequently, the SE of NUG increases asymptotically to that of RUG and AUG schemes, while in Fig. 8(c) the average SE increases when the blocklength increases. The reason is that when the A increases, the system moves away from the finite blocklength regime towards the Shannon rate [43]. Consequently, the spectral efficiency also increases. Again, the AUG scheme clearly outperforms all schemes while the AUG-DL scheme has a high accuracy prediction ability.

Figs. 9(a) and 9(b) show the effects of the reflection elements L_r with $L_t = 20$ and transmission element L_t with $L_r = 20$ on the average SE performance of all schemes. As the number of STAR-RIS elements increases, SE of all schemes improves due to finer control of electromagnetic waves, focusing signals more effectively towards the receiver, and forming narrower beams [44], which enhances SINR and SE. The impact of reflection elements on SE is more significant than transmission elements, as shown by lower SE when reflection elements decrease. The reason is that near users, closer to the STAR-RIS, have better channel conditions. Again, the AUG scheme has the highest SE performance among the considered schemes, and the AUG-DL shows good predictive ability.

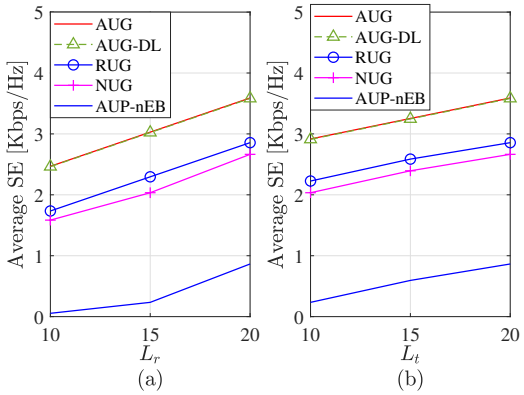

Fig. 9. Impact of the number reflection L_r and transmission elements L_t on the average SE.

Finally, we analyze the execution time of the conventional and DL approaches in Table V. When the number of users increases, the execution time of all approaches increases. In detail, the DL (AUG-DL) approach can guarantee an execution time of under one second. In contrast, the conventional approach (AUG) based on the Alg. 2 requires more time to obtain the optimal value due to some iteration to find the optimal solution. Thus, the proposed DL framework based on the CNN model has an excellent ability to predict optimal solutions and great promise for large-scale network scenarios.

TABLE V
EXECUTION TIME OF THE CONVENTIONAL AND DL APPROACHES

Number of users	12	24	36
AUG [seconds]	74	402	1,150
AUG-DL [seconds]	0.34	0.62	0.89

VII. CONCLUSIONS

We proposed an adaptive user grouping scheme for SPC in the STAR-RIS-assisted MIMO-NOMA system with SWIPT to improve SE performance under NL-EH circuit conditions. One near information user and one far information user with different channel conditions were optimally grouped while the energy users harvested the energy from the BS. We

formulated the SE maximization problem subject to mixed integer constraints. We then relaxed the integer part to continuous and decoupled the relaxed problem into phase shift and beamforming optimization sub-problems. To tackle the phase shift optimization sub-problem, we proposed a bisection search algorithm for its solution. Based on the optimal phase shift value, a low-complexity iterative algorithm based on the IA method was proposed to solve the beamforming optimization sub-problem, which guaranteed convergence to the local optima. Additionally, the DL framework based on the CNN model was developed to achieve real-time optimization via a quick-inference process. Simulation results illustrated the proposed AUG scheme's effectiveness in improving SE performance against benchmark schemes. Moreover, the AUG-DL scheme predicted the optimal value with high accuracy and in a short amount of time. Due to the high complexity of deploying energy splitting (ES)/time splitting (TS) protocols of STAR-RIS, we will continue to study the STAR-RISs-assisted MIMO-RSMA network with a novel DL technique and ES/TS protocols of STAR-RIS to solve the energy efficiency maximization (EEM) problem in beyond 5G wireless networks in the future works.

REFERENCES

[1] Y. L. Lee, D. Qin, L.-C. Wang, and G. H. Sim, "6G Massive Radio Access Networks: Key Applications, Requirements and Challenges," *IEEE Open J. Veh. Technol.*, vol. 2, no. October 2020, pp. 54–66, 2020.

[2] T. H. Vu, T.-V. Nguyen, D. B. Da Costa, and S. Kim, "Intelligent Reflecting Surface-Aided Short-Packet Non-Orthogonal Multiple Access Systems," *IEEE Trans. Veh. Technol.*, vol. 71, no. 4, pp. 4500–4505, 2022.

[3] D. D. Tran, S. K. Sharma, S. Chatzinotas, I. Woungang, and B. Ottersten, "Short-Packet Communications for MIMO NOMA Systems over Nakagami-m Fading: BLER and Minimum Blocklength Analysis," *IEEE Trans. Veh. Technol.*, vol. 70, no. 4, pp. 3583–3598, 2021.

[4] Y. Liu, X. Zhu, E. G. Lim, Y. Jiang, and Y. Huang, "Fast Iterative Semi-Blind Receiver for URLLC in Short-Frame Full-Duplex Systems With CFO," *IEEE J. Sel. Areas Commun.*, vol. 37, no. 4, pp. 839–853, 2019.

[5] X. Chen, F. K. Gong, G. Li, H. Zhang, and P. Song, "User Pairing and Pair Scheduling in Massive MIMO-NOMA Systems," *IEEE Commun. Lett.*, vol. 22, no. 4, pp. 788–791, 2018.

[6] T.-V. Nguyen, V. D. Nguyen, D. B. Da Costa, and B. An, "Hybrid User Pairing for Spectral and Energy Efficiencies in Multiuser MISO-NOMA Networks with SWIPT," *IEEE Trans. Commun.*, vol. 68, no. 8, pp. 4874–4890, Aug. 2020.

[7] R. H. Y. Perdana, T. V. Nguyen, and B. An, "Adaptive User Pairing in Multi-IRS-aided Massive MIMO-NOMA Networks: Spectral Efficiency Maximization and Deep Learning Design," *IEEE Trans. Commun.*, vol. 71, no. 7, pp. 4377–4390, 2023.

[8] R. H. Y. Perdana, T.-V. Nguyen, Y. Pramitarini, K. Shim, and B. An, "Deep Learning-based Spectral Efficiency Maximization in Massive MIMO-NOMA Systems with STAR-RIS," in *2023 Int. Conf. Artif. Intell. Inf. Commun.* Bali, Indonesia: IEEE, 2023, pp. 644–649.

[9] S. Dhok, and P. K. Sharma, "Rate-Splitting Multiple Access With STAR RIS Over Spatially-Correlated Channels," *IEEE Trans. Commun.*, vol. 70, no. 10, pp. 6410–6424, 2022.

[10] R. H. Y. Perdana, T.-V. Nguyen, and B. An, "A Deep Learning-Based Spectral Efficiency Maximization in Multiple Users Multiple STAR-RISs Massive MIMO-NOMA Networks," in *2023 Fourteenth Int. Conf. Ubiquitous Futur. Networks*. Paris, France: IEEE, 2023, pp. 675–680.

[11] T.-V. Nguyen, V.-D. Nguyen, D. B. D. Costa, H.-T. Thien, R. Q. Hu, and B. An, "Short-Packet Communications in Multi-Hop Networks with WET: Performance Analysis and Deep Learning-Aided Optimization," *IEEE Trans. Wirel. Commun.*, vol. 22, no. 1, p. 439, 2023.

[12] Y. Hu, Y. Zhu, M. C. Gursoy, and A. Schmeink, "SWIPT-Enabled relaying in IoT networks operating with finite blocklength codes," *IEEE J. Sel. Areas Commun.*, vol. 37, no. 1, pp. 74–88, 2019.

[13] B. Zhang, K. Wang, K. Yang, and G. Zhang, "IRS-Assisted Short Packet Wireless Energy Transfer and Communications," *IEEE Wirel. Commun. Lett.*, vol. 11, no. 2, pp. 303–307, 2022.

[14] F. Salehi, N. Neda, M.-H. Majidi, and H. Ahmadi, "Cooperative NOMA-Based User Pairing for URLLC: A Max-Min Fairness Approach," *IEEE Syst. J.*, vol. 16, no. 3, pp. 3833–3843, 2022.

[15] H. Ren, K. Wang, and C. Pan, "Intelligent Reflecting Surface-Aided URLLC in a Factory Automtion Scenario," *IEEE Trans. Commun.*, vol. 70, no. 1, pp. 707–723, 2022.

[16] J. Xu, L. Yuan, N. Yang, N. Yang, and Y. Guo, "Performance Analysis of STAR-IRS Aided NOMA Short-Packet Communications with Statistical CSI," *IEEE Trans. Veh. Technol.*, vol. 72, no. 9, pp. 12 385–12 390, 2023.

[17] T. H. Vu, T.-V. Nguyen, Q. V. Pham, D. B. da Costa, and A. Kim, "STAR-RIS-Enabled Short-Packet NOMA Systems," *IEEE Trans. Veh. Technol.*, vol. PP, pp. 1–6, 2023.

[18] T. Wang, F. Fang, and Z. Ding, "Joint Phase Shift and Beamforming Design in a Multi-User MISO STAR-RIS Assisted Downlink NOMA Network," *IEEE Trans. Veh. Technol.*, vol. 72, no. 7, pp. 9031–9043, 2023.

[19] R. H. Y. Perdana, T. V. Nguyen, and B. An, "Deep neural network design with SLNR and SINR criterions for downlink power allocation in multi-cell multi-user massive MIMO systems," *ICT Express*, vol. 9, no. 2, pp. 228–234, 2023.

[20] J. Zhang, W. Xia, M. You, G. Zheng, S. Lambotharan, and K. K. Wong, "Deep Learning Enabled Optimization of Downlink Beamforming under Per-Antenna Power Constraints: Algorithms and Experimental Demonstration," *IEEE Trans. Wirel. Commun.*, vol. 19, no. 6, pp. 3738–3752, 2020.

[21] M. Alsenwi, N. H. Tran, M. Bennis, S. R. Pandey, A. K. Bairagi, and C. S. Hong, "Intelligent Resource Slicing for eMBB and URLLC Coexistence in 5G and Beyond: A Deep Reinforcement Learning Based Approach," *IEEE Trans. Wirel. Commun.*, vol. 20, no. 7, pp. 4585–4600, 2021.

[22] Y. Huang, Y. Thomas Hou, and W. Lou, "DELUXE: A DL-Based Link Adaptation for URLLC/eMBB Multiplexing in 5G NR," *IEEE J. Sel. Areas Commun.*, vol. 40, no. 1, pp. 143–162, 2022.

[23] T. D. Ponnimbaduge Perera, D. N. K. Jayakody, S. K. Sharma, S. Chatzinotas, and J. Li, "Simultaneous Wireless Information and Power Transfer (SWIPT): Recent Advances and Future Challenges," *IEEE Commun. Surv. Tutorials*, vol. 20, no. 1, pp. 264–302, 2018.

[24] B. R. Marks and G. P. Wright, "Technical Note—A General Inner Approximation Algorithm for Nonconvex Mathematical Programs," *Oper. Res.*, vol. 26, no. 4, pp. 681–683, Aug. 1978.

[25] T. L. Marzetta, E. G. Larsson, H. Yang, and H. Q. Ngo, *Fundamental of Massive MIMO*. New York: Cambridge University Press, 2016.

[26] E. Bjornson and L. Sanguinetti, "Rayleigh Fading Modeling and Channel Hardening for Reconfigurable Intelligent Surfaces," *IEEE Wirel. Commun. Lett.*, vol. 10, no. 4, pp. 830–834, 2021.

[27] S. Yang, Z. Ding, and H. Zhu, "STAR-RIS Aided Multi-Antenna NOMA Downlink and Uplink Transmissions: A Low-Complexity Approach," *IEEE Trans. Wirel. Commun.*, vol. PP, p. 1, 2024.

[28] Q. Wu and R. Zhang, "Towards Smart and Reconfigurable Environment: Intelligent Reflecting Surface Aided Wireless Network," *IEEE Commun. Mag.*, vol. 58, no. 1, pp. 106–112, nov 2020.

[29] T.-H. Vu, T.-V. Nguyen, D. B. da Benevides, and S. Kim, "Reconfigurable Intelligent Surface-Aided Cognitive NOMA Networks : Performance Analysis and Deep Learning Evaluation," *IEEE Trans. Wirel. Commun.*, vol. 21, no. 12, pp. 10 662–10 677, 2022.

[30] T. N. Do, G. Kaddoum, T. L. Nguyen, D. B. da Costa, and Z. J. Haas, "Multi-RIS-aided Wireless Systems: Statistical Characterization and Performance Analysis," *IEEE Trans. Commun.*, vol. 6778, no. c, pp. 1–18, 2021.

[31] Z. Xie, W. Yi, X. Wu, Y. Liu, and A. Nallanathan, "STAR-RIS Aided NOMA in Multicell Networks: A General Analytical Framework With Gamma Distributed Channel Modeling," *IEEE Trans. Commun.*, vol. 70, no. 8, pp. 5629–5644, 2022.

[32] E. Boshkovska, D. W. K. Ng, N. Zlatanov, and R. Schober, "Practical non-linear energy harvesting model and resource allocation for SWIPT systems," *IEEE Commun. Lett.*, vol. 19, no. 12, pp. 2082–2085, 2015.

[33] X. Gao, Y. Liu, X. Liu, and Z. Qin, "Resource Allocation in IRSs Aided MISO-NOMA Networks: A Machine Learning Approach," in *2020 IEEE Glob. Commun. Conf.*, Taipei, Taiwan, 2020.

[34] Z. Yang, P. Xu, G. Chen, Y. Wu, and Z. Ding, "Performance Analysis of IRS-Assisted NOMA Networks With Randomly Deployed Users," *IEEE Syst. J.*, pp. 1–12, 2022.

[35] Z. Ding, P. Fan, and H. V. Poor, "Impact of User Pairing on 5G Nonorthogonal Multiple-Access Downlink Transmissions," *IEEE Trans. Veh. Technol.*, vol. 65, no. 8, pp. 6010–6023, Aug. 2016.

[36] B. Makki, T. Svensson, and M. Zorzi, "Wireless Energy and Information Transmission Using Feedback: Infinite and Finite Block-Length Analysis," *IEEE Trans. Commun.*, vol. 64, no. 12, pp. 5304–5318, 2016.
[37] F. Fang, B. Wu, S. Fu, Z. Ding, and X. Wang, "Energy-Efficient Design of STAR-RIS Aided MIMO-NOMA Networks," *IEEE Trans. Commun.*, vol. 71, no. 1, pp. 498–511, 2023.
[38] V. D. Nguyen, T. Q. Duong, H. D. Tuan, O. S. Shin, and H. V. Poor, "Spectral and Energy Efficiencies in Full-Duplex Wireless Information and Power Transfer," *IEEE Trans. Commun.*, vol. 65, no. 5, pp. 2220–2233, May 2017.
[39] A. Beck, A. Ben-Tal, and L. Tetruashvili, "A sequential parametric convex approximation method with applications to nonconvex truss topology design problems," *J. Glob. Optim.*, vol. 47, no. 1, pp. 29–51, July 2010.
[40] V. D. Nguyen, H. D. Tuan, T. Q. Duong, H. V. Poor, and O. S. Shin, "Precoder design for signal superposition in MIMO-NOMA multicell networks," *IEEE J. Sel. Areas Commun.*, vol. 35, no. 12, pp. 2681–2695, Dec. 2017.
[41] A. A. Nasir, H. D. Tuan, H. H. Nguyen, M. Debbah, and H. V. Poor, "Resource Allocation and Beamforming Design in the Short Blocklength Regime for URLLC," *IEEE Trans. Wirel. Commun.*, vol. 20, no. 2, pp. 1321–1335, 2021.
[42] Y. Pramitarini, R. H. Y. Perdana, K. Shim, and B. An, "Opportunistic Scheduling Scheme to Improve Physical-Layer Security in Cooperative NOMA System : Performance Analysis and Deep Learning Design," *IEEE Access*, vol. 12, pp. 58 454–58 472, 2024.
[43] R. Hashemi, S. Ali, N. H. Mahmood, and M. Latva-Aho, "Average Rate and Error Probability Analysis in Short Packet Communications over RIS-Aided URLLC Systems," *IEEE Trans. Veh. Technol.*, vol. 70, no. 10, pp. 10 320–10 334, 2021.
[44] C. Huang, R. Mo, and C. Yuen, "Reconfigurable Intelligent Surface Assisted Multiuser MISO Systems Exploiting Deep Reinforcement Learning," *IEEE J. Sel. Areas Commun.*, vol. 38, no. 8, pp. 1839–1850, 2020.

Ridho Hendra Yoga Perdana (Graduate Student Member, IEEE) received the B.S degree in telecommunications engineering from Electronic Engineering Polytechnic Institute of Surabaya, Surabaya, Indonesia, in 2012 and the M.S. degree in electrical engineering from Institut Teknologi Sepuluh Nopember (ITS), Surabaya, Indonesia in 2014. He is currently pursuing the Ph.D. degree with the Department of Software and Communications Engineering, Graduate School, Hongik University, Sejong, South Korea. His main research interests include mathematical modeling of 5G networks and machine learning for wireless communications. He received the Best Paper Award of the IEEE International Conference on Artificial Intelligence in Information and Communication 2024.

Toan-Van Nguyen (Member, IEEE) received the B.S. degree in Electronics and Telecommunications Technology and the M.Eng. degree in Electronic Engineering from HCMC University of Technology and Education, Vietnam, in 2011 and 2014, respectively, and the Ph.D. degree in Electronics and Computer Engineering from Hongik University, South Korea, in 2021. He is currently a Postdoctoral Researcher in the Department of Electrical and Computer Engineering at San Diego State University, CA 92182, USA. His current research focuses on data detection and channel estimation of MIMO systems, and optimization/machine learning for wireless communications.

Yushintia Pramitarini (Graduate Student Member, IEEE) received the B.S degree in telecommunications engineering from Electronic Engineering Polytechnic Institute of Surabaya, Surabaya, Indonesia, in 2011 and the M.S. degree in electrical engineering from Institut Teknologi Sepuluh Nopember (ITS), Surabaya, Indonesia, in 2013. She is currently pursuing the Ph.D. degree in the Department of Software and Communications Engineering, Graduate School, Hongik University, Sejong, Republic of Korea. Her current research activity is focused on mobile wireless networks, clustering, QoS routing & QoS multicast routing, machine learning applications, and physical layer security(PLS). In 2024, she received the IEEE International Conference on Artificial Intelligence in Information and Communication Best Paper Award.

Duy H. N. Nguyen (Senior Member, IEEE) received the B.Eng. degree (Hons.) from the Swinburne University of Technology, Hawthorn, VIC, Australia, in 2005, the M.Sc. degree from the University of Saskatchewan, Saskatoon, SK, Canada, in 2009, and the Ph.D. degree from McGill University, Montréal, QC, Canada, in 2013, all in electrical engineering. From 2013 to 2015, he held a joint appointment as a Research Associate with McGill University and a Post-doctoral Research Fellow with the Institut National de la Recherche Scientifique, Université du Québec, Montréal, QC, Canada. He was a Research Assistant with the University of Houston, Houston, TX, USA, in 2015, and a Post-doctoral Research Fellow with the University of Texas at Austin, Austin, TX, USA, in 2016. He is an Associate Professor at the Department of Electrical and Computer Engineering, San Diego State University, San Diego, CA, USA. His current research interests include resource allocation in wireless networks, signal processing for communications, convex optimization, game theory, and machine learning. Dr. Nguyen was a recipient of the Australian Development Scholarship, the FRQNT Doctoral and Post-doctoral Fellowship, and the NSERC Post-doctoral Fellowship. He received a Best Paper Award at the 2020 IEEE International Conference on Communications (ICC). He is currently an Associate Editor for the *IEEE Open Journal of the Communications Society.*

Beongku An (Senior Member, IEEE) received the B.S. degree in electronic engineering from Kyungpook National University, Republic of Korea, in 1988, the M.S. degree in electrical engineering from Polytechnic University (NYU), NY, USA, in 1996 and Ph.D. degree in electrical engineering from New Jersey Institute of Technology (NJIT), NJ, USA, in 2002, respectively. After graduation, he joined the Faculty of the Department of Software and Communications Engineering, Hongik University, Republic of Korea, where he is currently a Professor. From 1989 to 1993, he was a senior researcher in RIST, Republic of Korea. He was a president of IEIE Computer Society in 2012 and also worked as a General Chair in the International Conference (ICGHIT) from 2013 to 2017. His current research interests include mobile wireless networks and communications such as ad-hoc & sensor networks, cognitive radio networks, cellular networks, and IoT. In particular, he is interested in cooperative transmission, QoS routing & QoS multicast routing, energy harvesting, physical layer security(PLS), visible light communication(VLC), cross-layer technology, 5G/Beyond 5G, Machine Learning/Deep Learning applications. Professor An was listed in Marquis Who's Who in Science and Engineering, and Marquis Who's Who in the World, respectively.